Kasdi Merbah University of Ouargla
Faculty of Mathematics and Material Sciences

N° d'ordre :
N° de série :

Department of Mathematics:
MASTER
Major: Mathematics
Specialization: Modeling and Numerical Analysis
Presented by: Chaima Khabbar

Theme:

Inverse Identification of Space-Dependent Fractional Order in Subdiffusion Equations

Defended on: 04/06/2026

Jury members:

Mr.	**Merabet Ismail**	Prof. Kasdi Merbah University-Ouargla	Chairman
Mr.	**Bensayah Abdallah**	Prof. Kasdi Merbah University-Ouargla	Examiner
Ms.	**Messaoudi Djemaa**	M.C.A. Kasdi Merbah University-Ouargla	Supervisor

Academic Year: 2025-2026

Dedication

In the name of Allah, the Most Gracious, the Most Merciful

Peace and blessings be upon the most honorable of prophets and messengers

To the heartbeat of my heart, the secret of my existence, and my happiness: to my dear **"Mother"**

To the light that illuminated my path, to the dear one whose name I carry with pride: **"Father"**

To my supporters and those who stood by me, my siblings: **Fatima Al-Zahra, Hicham, Oussama, Okba, and Zakaria**

To the source of joy and delight, the grandchildren**Chahd, Assil, Tasnim, and Anas**

To the one whom Allah chose to be my other half: my **"Fiance"**

To the beloved whose body has departed but whose memory remains, my first teacher: **"Khalou Kadour"**, may Allah have mercy on him

To those who shared my joy and sadness, my friends: **Sawsan, Marwa, and Wafaa**

To everyone who helped me in making this work a success

I dedicate this work

Finally

I ask Allah that this work be a benefit to me and others, and that it be a beginning of goodness for me in my future path.

Acknowledgement

I extend my highest sentiments of gratitude and deepest expressions of thanks to my supervisor, **Dr. Djemaa Messaoudi** , who was an exemplary guide and supporter. She spared neither her time nor her knowledge, and her direction was a beacon that illuminated my path, while her support served as a powerful impetus enabling me to overcome difficulties.

I am also pleased to express my sincere appreciation to the esteemed members of the thesis committee:

Prof. Abdallah Bensayah and Prof. Ismail Merabet

for their gracious acceptance to read and evaluate this dissertation, and for their valuable discussions, which have added immensely to my work.

Nor do I forget to thank all the professors of the **Department of Mathematics** at the **University of Kasdi Merbah Ouargla**, who contributed to my academic formation throughout my years of study.

May Allah reward them all with the best of rewards.

Contents

List of Tables

List of Figures

Notations

- ∇u: Gradient of u.
- Δu: Laplace operator.
- V': Dual space of V.
- $\mathcal{L}(X, Y)$: Space of bounded linear operators from X to Y.
- $(\cdot, \cdot)$: Inner product in $L^2(\Omega)$.
- $\langle \cdot, \cdot \rangle$: Duality pairing between V' and V.
- $L^p(\Omega)$: Lebesgue space.
- $W^{k,p}(\Omega)$: Sobolev space.
- $H^k(\Omega) = W^{k,2}(\Omega)$: Sobolev Hilbert space.
- $H_0^1(\Omega)$: Closure of $C_c^\infty(\Omega)$ in $H^1(\Omega)$.
- $\widetilde{H}^s(\Omega)$: Fractional Sobolev space.
- $\|\cdot\|_X$: Norm in the space X.
- $L^p(0, T; B) = \left\{ u : [0, T] \to B \;\middle|\; \int_0^T \|u(t)\|_B^p \, dt < \infty \right\}$: Bochner space.

- $H^1(0,T;B) = \left\{u \in L^2(0,T;B) \;\middle|\; \partial_t u \in L^2(0,T;B)\right\}$: Bochner–Sobolev space.
- $L^2(0,T;L^2(\Omega))$: Space of square-integrable functions on $\Omega \times (0,T)$.
- $L^2(0,T;H_0^1(\Omega))$: Space of functions in $L^2(0,T)$ with values in $H_0^1(\Omega)$.

Introduction

Inverse problems constitute a fundamental area of applied mathematics, where the objective is to determine unknown causes, parameters, or system characteristics from indirect observations. Unlike direct problems, in which the system parameters are known and the corresponding response is computed, inverse problems seek to infer hidden information from measured data. Such problems arise naturally in numerous scientific and engineering applications where direct measurements are either difficult, expensive, or impossible to obtain.

The study of inverse problems dates back to the beginning of the twentieth century [13]. Early investigations were primarily motivated by challenges in the physical sciences, including quantum scattering theory, geophysical prospecting, seismology, and potential theory. These pioneering works established the theoretical foundations for recovering unknown quantities from observed data and initiated the development of mathematical techniques that remain influential today. With the rapid advancement of computational methods and high-performance computing during the second half of the twentieth century, inverse problems evolved into a major research field with applications extending far beyond physics [19]. Nowadays, inverse problem methodologies play a crucial role in medical imaging, non-destructive testing, environmental monitoring, remote sensing, and many other technological domains. Owing to their broad range of applications, inverse problems

continue to attract considerable attention from researchers. Significant progress has been achieved in both the theoretical analysis and numerical treatment of inverse problems, particularly in the identification of unknown parameters and coefficients in mathematical models [1, 29, 30, 31, 34]. These advances have contributed to the development of reliable techniques for recovering unknown quantities from indirect and noisy measurements.

At the same time, the increasing complexity of modern scientific models has highlighted the limitations of classical differential equations in describing processes exhibiting memory effects and nonlocal interactions. In this context, fractional calculus has emerged as a powerful mathematical framework capable of capturing such phenomena more accurately than traditional integer-order models. In particular, fractional differential equations have proven highly effective in modeling anomalous diffusion processes, where particle transport deviates from the classical Brownian motion assumption [32]. Unlike standard diffusion, anomalous diffusion exhibits long-range temporal memory and spatial heterogeneity, characteristics that are frequently observed in biological tissues, porous media, viscoelastic materials, and complex physical systems [28].

Recent developments have further demonstrated that many real-world systems cannot be adequately represented by a single constant fractional order. Instead, the diffusion dynamics may vary spatially due to heterogeneous material properties or varying environmental conditions. This observation has motivated the introduction of variable-order fractional models, in which the fractional order depends on the spatial variable. Such models provide a more realistic description of heterogeneous media and offer greater flexibility in representing complex diffusion mechanisms. Significant progress has been made in the mathematical analysis of these models, including studies on the existence, uniqueness, and regularity of solutions [18]. Nevertheless, many theoretical and computational challenges remain open, particularly in the context of inverse parameter identification.

One of the most important challenges concerns the recovery of the spatially dependent fractional order $\alpha(x)$ from available observations of the system state. This leads to an inverse coefficient problem whose objective is to identify the fractional-order distribution governing the diffusion process. Such problems are generally ill-posed in the sense of

Hadamard, since small perturbations in the measured data may produce large variations in the reconstructed parameter [13]. Consequently, obtaining stable and reliable solutions requires the development of appropriate mathematical frameworks, regularization techniques, and efficient numerical algorithms.

One of the main contributions of this thesis is the investigation of an inverse problem for a variable-order time-fractional diffusion equation, where the fractional order varies spatially across the domain. The reconstruction problem is formulated within an optimization framework incorporating Tikhonov regularization, adjoint-based gradient computation, and finite element discretization to obtain stable numerical solutions from noisy data. In addition, Physics-Informed Neural Networks (PINNs) are employed as a mesh-free alternative approach. A comparative study between the optimization-based method and PINNs is conducted, providing insight into their respective advantages and limitations for the identification of spatially varying fractional orders.

The thesis is organized as follows.

- **Chapter One** introduces the mathematical background and theoretical framework required for the study of the proposed inverse problem. It presents the fundamental concepts of inverse problems and variable-order fractional diffusion models, discusses their practical applications, and formulates the forward and inverse problems under consideration. The chapter also introduces the variable-order fractional operators, the Tikhonov regularization framework, and the main functional analysis tools used throughout the thesis.

- **Chapter Two** is devoted to the analysis of the forward problem. We investigate the well-posedness of the variable-order fractional subdiffusion equation by establishing existence, uniqueness, and regularity results for the corresponding solution. These properties provide the theoretical foundation required for the subsequent inverse analysis.

- **Chapter Three** focuses on the inverse identification problem. The reconstruction of the unknown fractional order $\alpha(x)$ is formulated as an optimization problem. To

address the ill-posedness of the problem, Tikhonov regularization is incorporated into the objective functional, and the associated optimality conditions are derived.

- **Chapter Four** is dedicated to the numerical treatment of the inverse problem. Numerical algorithms are developed and implemented to reconstruct the unknown coefficient from synthetic noisy data. Several numerical experiments are presented to assess the accuracy, stability, and robustness of the proposed methodology. Furthermore, the obtained results are compared with those generated by Physics-Informed Neural Networks (PINNs), highlighting the advantages and limitations of both approaches.

Chapter 1

Mathematical Background and Problem Setting

1.1 Introduction and Motivation

Fractional differential equations have emerged as powerful mathematical tools for modeling complex dynamical processes exhibiting memory and hereditary effects. Unlike classical differential equations, which describe the evolution of a system solely through its current state, fractional models incorporate information from the past history of the process. This nonlocal behavior makes them particularly suitable for representing a wide range of physical phenomena in which memory effects play a fundamental role.

Over the last few decades, fractional calculus has found numerous applications in physics, engineering, biology, geosciences, and materials science. In particular, Fractional diffusion models have been successfully employed to describe anomalous transport phenomena in heterogeneous media [6], where classical diffusion models fail to reproduce experimentally observed behaviors. Examples include contaminant transport in porous formations, heat transfer in composite materials, diffusion in biological tissues, and vis-

coelastic deformation of geomaterials.

Although constant-order fractional models provide a significant improvement over classical models, they still assume that the same diffusion mechanism governs the entire spatial domain. In many practical situations, however, the physical properties of the medium vary from one location to another. Such heterogeneities may lead to spatially varying memory effects and transport behaviors that cannot be adequately represented by a single fractional order.

To overcome this limitation, variable-order fractional models have been introduced. In these models, the fractional order is allowed to depend on spatial position, time, or both. The resulting framework offers greater flexibility and enables a more realistic representation of heterogeneous systems. In particular, a space-dependent fractional order $\alpha(x)$ can be interpreted as a parameter describing local diffusion characteristics and memory properties of the medium. Recently, Related inverse problems involving variable-order time-fractional diffusion equations have been studied in [7, 12].

In many applications, the fractional order is not directly accessible through measurements and must therefore be inferred from observed data. This naturally leads to an inverse problem. Rather than determining the state variable for a known model, the objective is to recover an unknown parameter that characterizes the underlying physical process. In the context of variable-order fractional diffusion equations, the reconstruction of the spatially varying fractional order provides valuable information about the internal structure and transport properties of the medium.

Inverse problems of this type are generally challenging because they are often ill-posed in the sense of Hadamard. Small perturbations in measurement data may produce large variations in the reconstructed parameter, making the identification process highly sensitive to noise. Consequently, suitable regularization techniques are required to ensure stability and reliability of the reconstruction.

The present thesis is devoted to the analysis and numerical solution of an inverse problem associated with a variable-order time-fractional diffusion equation. The primary objective is to reconstruct an unknown space-dependent fractional order from noisy ob-

servations of the state variable. To achieve this goal, the problem is formulated as a Tikhonov regularized optimization problem, and both theoretical and numerical aspects of the reconstruction process are investigated.

This chapter introduces the mathematical background required throughout the thesis. We first discuss the role of inverse problems in fractional diffusion models and review several motivating applications. We then formulate the forward and inverse problems under consideration, introduce the variable-order fractional operators employed in the model, and present the regularization framework and mathematical tools that will be used in the subsequent chapters.

1.2 Inverse problems in fractional diffusion models

Mathematical models are widely used to describe physical phenomena through differential equations. In many situations, the parameters appearing in these models are known, and the objective is to determine the corresponding state variable. Such problems are commonly referred to as forward problems. In contrast, an inverse problem aims to recover unknown parameters or characteristics of a system from indirect observations of its response.

Inverse problems arise naturally in numerous scientific and engineering applications [16], including medical imaging, geophysical exploration, non-destructive testing, environmental monitoring, and material characterization. Their objective is often to identify quantities that cannot be measured directly but strongly influence the observed behavior of the system.

Definition 1.2.1 (Inverse problem) *Let $F(p) = z$, where p denotes an unknown parameter, z represents the available observational data, and F is the parameter-to-state map associated with the governing model. The inverse problem consists of determining the parameter p from the measured data z.*

In the context of diffusion phenomena, inverse problems may involve the identification of diffusion coefficients, source terms, initial conditions, boundary conditions, or fractional

orders. Such problems are of considerable practical importance because the unknown parameters often contain valuable information about the internal properties of the medium under investigation.

Fractional diffusion models introduce additional challenges due to the nonlocal nature of fractional operators. The solution at a given time depends on the entire history of the process, leading to a highly nonlinear relationship between the observations and the unknown parameters. Consequently, inverse problems associated with fractional differential equations are generally more difficult than their classical counterparts.

A fundamental feature of inverse problems is that they are frequently ill-posed in the sense of Hadamard. This means that at least one of the following properties may fail: existence of a solution, uniqueness of the solution, or continuous dependence of the solution on the data. As a result, small measurement errors may produce large variations in the reconstructed parameter. A comprehensive introduction to the mathematical and computational aspects of inverse problems can be found in [3].

Definition 1.2.2 (Hadamard well-posedness) *A mathematical problem is said to be well-posed if:*

1. *a solution exists;*
2. *the solution is unique;*
3. *the solution depends continuously on the data.*

If one of these conditions is not satisfied, the problem is said to be ill-posed [11].

1.2.1 Examples of well-posed problems

1. Let us consider the Dirichlet problem for Laplace's equation on a bounded domain

$$\begin{cases} -\Delta u = f & \text{in } \Omega \subset \mathbb{R}^d, \\ u = g & \text{on } \partial\Omega. \end{cases} \tag{1.1}$$

For every $f \in H^{-1}(\Omega)$ and $g \in H^{1/2}(\partial\Omega)$, then problem (1.1) is well posed by the Lax-Milgram theorem (for the proof, see [4]).

2. Let us consider the heat equation with initial and boundary conditions

$$\begin{cases} \partial_t u - \Delta u = f & \text{in } \Omega \times (0,T], \\ u(x,0) = u_0(x) & \text{in } \Omega, \\ u = 0 & \text{on } \partial\Omega \times (0,T]. \end{cases} \tag{1.2}$$

For every $u_0 \in L^2(\Omega)$ and $f \in L^2(0,T;L^2(\Omega))$, problem (1.2) admits a unique solution in $L^2(0,T;H_0^1(\Omega)) \cap C([0,T];L^2(\Omega))$ by the Galerkin method (see the proof in ([23]). Hence, problem 1.2 is well-posed.

3. Let us consider the constant-order fractional diffusion problem

$$\begin{cases} \partial_t^\alpha u - \Delta u = f & \text{in } \Omega \times (0,T], \\ u(x,0) = u_0(x) & \text{in } \Omega, \\ u = 0 & \text{on } \partial\Omega \times (0,T], \end{cases} \tag{1.3}$$

where $0 < \alpha < 1$ and ∂_t^α denotes the Caputo fractional derivative. For every $u_0 \in L^2(\Omega)$ and $f \in L^2(0,T;L^2(\Omega))$, problem (1.3) admits a unique solution (see the proof in [27]). Consequently, problem (1.3) is well-posed.

To overcome these difficulties, regularization techniques are commonly employed. These methods stabilize the reconstruction process by incorporating additional information or constraints on the unknown parameter. Among the various regularization approaches available in the literature, Tikhonov regularization remains one of the most widely used due to its mathematical simplicity and robustness.

In this thesis, we consider the inverse problem of recovering an unknown space-dependent fractional order from measurements of the state variable governed by a variable-order fractional diffusion equation. The fractional order serves as a parameter characterizing the local diffusion behavior of the medium, and its identification provides valuable insight into the underlying physical process.

1.3 Applications of variable-order fractional inverse problems

The identification of unknown parameters from indirect measurements plays a fundamental role in many areas of science and engineering. In variable-order fractional diffusion models, the fractional order is often associated with the local memory and transport properties of the medium. Consequently, reconstructing a space-dependent fractional order from observational data provides valuable information about the internal structure and physical characteristics of the system.

One important application arises in subsurface flow and contaminant transport. Geological formations are typically heterogeneous, with spatial variations in permeability and porosity that significantly influence diffusion processes. Variable-order fractional models provide a flexible framework for describing such heterogeneities, and the reconstruction of the fractional order can assist in the characterization of underground reservoirs and aquifers.

Another important application concerns biological tissues. Diffusion processes in living tissues are strongly affected by complex cellular structures and heterogeneous microenvironments. The identification of a spatially varying fractional order from measurement data may provide useful information about tissue properties and can contribute to the detection of structural abnormalities.

Variable-order fractional models are also widely employed in viscoelasticity and material science. The fractional order often reflects the local rheological behavior of a material and may vary due to aging, damage, or manufacturing defects. Recovering this parameter from experimental observations therefore offers a non-destructive means of assessing material integrity and performance.

Variable-order fractional models have been successfully applied in geotechnical engineering, viscoelastic materials, creep analysis, and underground structures [8, 17, 20, 21, 22, 40, 41, 42, 45].

These examples illustrate that the fractional order is not merely a mathematical pa-

rameter but often possesses a direct physical interpretation. Therefore, its identification from observational data constitutes an important inverse problem with numerous practical applications.

1.4 Problem statement

Let $\Omega \subset \mathbb{R}^d$, $d = 1, 2, 3$, be a bounded domain with boundary $\partial\Omega$, and let $T > 0$ denote a fixed final time. We consider the variable-order time-fractional diffusion equation

$$\begin{cases} \partial_t^{\alpha(x)} u(x,t) - \Delta u(x,t) = f(x,t), & (x,t) \in \Omega \times (0,T], \\ u(x,0) = u_0(x), & x \in \Omega, \\ u(x,t) = 0, & (x,t) \in \partial\Omega \times (0,T], \end{cases} \tag{1.4}$$

where $u = u(x,t)$ denotes the state variable, f is a given source term, u_0 is the initial condition, and $\partial_t^{\alpha(x)}$ represents a variable-order fractional derivative in time. The function $\alpha(x)$ is assumed to satisfy

$$0 < \alpha_{\min} \leq \alpha(x) \leq \alpha_{\max} < 1, \qquad x \in \Omega,$$

so that the model remains in the subdiffusive regime.

Throughout this work, the fractional order is assumed to belong to the admissible set which will see in details in next sections,

$$\mathcal{A} = \left\{ \alpha \in H^1(\Omega) : \alpha_{\min} \leq \alpha(x) \leq \alpha_{\max} \text{ a.e. in } \Omega \right\}.$$

For a given fractional-order distribution $\alpha \in \mathcal{A}$, problem (1.4) constitutes the forward problem and determines the corresponding state solution u.

The main objective of this thesis is to identify the unknown function $\alpha(x)$ from measurements of the state variable. More precisely, we assume that observational data are available in the form $z^\delta = u + \xi$, where ξ represents measurement noise satisfying

$$\|\xi\|_{L^2(0,T;L^2(\Omega))} \leq \delta,$$

with $\delta > 0$ denoting the noise level.

The inverse problem under consideration can therefore be stated as follows:

Given the observational data z^δ, determine the unknown space-dependent fractional order $\alpha(x)$ appearing in the variable-order diffusion equation (1.4).

Since this inverse problem is generally ill-posed, regularization techniques are required to obtain stable and reliable reconstructions. The corresponding regularized formulation will be introduced in Section 1.6.

1.5 Variable-order fractional calculus

Fractional calculus extends the classical concepts of differentiation and integration to non-integer orders. In recent years, fractional differential operators have become important tools for modeling complex processes involving memory and hereditary effects. In particular, variable-order fractional operators provide additional flexibility by allowing the order of differentiation to vary throughout the domain.

In this work, we employ the variable-order Caputo fractional derivative. Let $\alpha(x) \in (0,1)$ and let $u = u(x,t)$ be sufficiently smooth. The variable-order Caputo derivative of u is defined by

$$\partial_t^{\alpha(x)} u(x,t) = \frac{1}{\Gamma(1-\alpha(x))} \int_0^t (t-s)^{-\alpha(x)} \frac{\partial u}{\partial s}(x,s)\, ds, \tag{1.5}$$

where $\Gamma(\cdot)$ denotes the Gamma function.

When the fractional order is constant, that is, $\alpha(x) \equiv \alpha$, the definition (1.5) reduces to the classical Caputo fractional derivative. The spatial dependence of the order allows the model to capture heterogeneous memory effects and spatially varying diffusion mechanisms.

The Caputo derivative is particularly attractive for physical applications because it permits the use of classical initial conditions expressed in terms of integer-order derivatives. For this reason, it is widely used in the modeling of diffusion, transport, and viscoelastic phenomena.

Throughout this thesis, the variable-order Caputo derivative serves as the fundamental operator in the mathematical model and plays a central role in both the theoretical analysis and the numerical reconstruction of the unknown fractional order.

Lemma 1.5.1 (Properties of variable-order fractional derivatives) *For $\alpha(x) \in \mathcal{A}$:*

1. ***Reduction to constant case**: If $\alpha(x) \equiv \alpha_0$ constant, then $\partial_t^{\alpha(x)} = \partial_t^{\alpha_0}$*
2. ***Positivity**: For $u \in L^2(0,T;H_0^1(\Omega))$ with $u(0) = 0$ and sufficiently regular temporal behavior,*
$$\int_0^T (\partial_t^{\alpha(x)} u(t), u(t)) dt \geq 0 \tag{1.6}$$
3. ***Composition rule**: For $\alpha(x), \beta(x) \in \mathcal{A}$ with $\alpha(x) + \beta(x) < 1$,*
$$\partial_t^{\alpha(x)} \partial_t^{\beta(x)} u = \partial_t^{\alpha(x)+\beta(x)} u + R(x,t)$$
where $R(x,t)$ involves derivatives of α, β and is of lower order.

Proof.

1. **Reduction to constant case**: According to Caputo's definition of the fractional derivative, we have:
$$\partial_t^{\alpha(x)} u(x,t) = \frac{1}{\Gamma(1-\alpha(x))} \int_0^t (t-\tau)^{-\alpha(x)} \frac{\partial u(x,\tau)}{\partial \tau} d\tau$$
Substitute $\alpha(x) = \alpha_0$:
$$\partial_t^{\alpha_0} u(x,t) = \frac{1}{\Gamma(1-\alpha_0)} \int_0^t (t-\tau)^{-\alpha_0} \frac{\partial u(x,\tau)}{\partial \tau} d\tau$$
$$= \partial_t^{\alpha_0} u(x,t)$$
2. **Positivity**: According to Caputo's definition of the fractional derivative, we have:
$$\partial_t^{\alpha(x)} u(x,t) = \frac{1}{\Gamma(1-\alpha(x))} \int_0^t (t-s)^{-\alpha(x)} \frac{\partial u}{\partial s}(x,s)\, ds$$
Where:
   - $0 < \alpha(x) < 1$

- $u(x,0) = 0$
- $u(x,T) = 0$ (or $T \to \infty$)
- $u \in H_0^1(0,T;L^2(\Omega))$

$$I = \int_0^T \left(\partial_t^{\alpha(x)} u(x,t), u(x,t)\right) dt$$

where $(\cdot,\cdot)$ is the inner product in $L^2(\Omega)$.

$$I = \int_0^T \int_\Omega \partial_t^{\alpha(x)} u(x,t)\, u(x,t)\, dx\, dt$$

Substitute the definition

$$I = \int_0^T \int_\Omega \left[\frac{1}{\Gamma(1-\alpha(x))} \int_0^t (t-s)^{-\alpha(x)} \frac{\partial u}{\partial s}(x,s)\, ds\right] u(x,t)\, dx\, dt$$

Factor out the constant

$$I = \int_\Omega \frac{1}{\Gamma(1-\alpha(x))} \left[\int_{t=0}^T \int_{s=0}^t (t-s)^{-\alpha(x)} \frac{\partial u}{\partial s}(x,s)\, u(x,t)\, ds\, dt\right] dx$$

The region of integration is $0 \le s \le t \le T$. Using Fubini's theorem

$$\int_{t=0}^T \int_{s=0}^t F(t,s)\, ds\, dt = \int_{s=0}^T \int_{t=s}^T F(t,s)\, dt\, ds$$

Applying this

$$\int_0^T \int_0^t (t-s)^{-\alpha(x)} \frac{\partial u}{\partial s}(x,s)\, u(x,t)\, ds\, dt = \int_0^T \int_s^T (t-s)^{-\alpha(x)} u(x,t)\, dt\, \frac{\partial u}{\partial s}(x,s)\, ds$$

Therefore

$$I = \int_\Omega \frac{1}{\Gamma(1-\alpha(x))} \left[\int_{s=0}^T \int_{t=s}^T (t-s)^{-\alpha(x)} u(x,t)\, dt\, \frac{\partial u}{\partial s}(x,s)\, ds\right] dx$$

We take

$$J(x,s) = \int_s^T (t-s)^{-\alpha(x)} u(x,t)\, dt$$

So

$$I = \int_\Omega \frac{1}{\Gamma(1-\alpha(x))} \left[\int_0^T J(x,s)\, \frac{\partial u}{\partial s}(x,s)\, ds\right] dx$$

Integrate by parts with respect to s:

$$\int_0^T J(x,s)\,\frac{\partial u}{\partial s}(x,s)\,ds = [J(x,s)u(x,s)]_{s=0}^{s=T} - \int_0^T \frac{\partial J}{\partial s}(x,s)u(x,s)ds$$

Since $J(x,T)=0$ and $u(x,0)=0$:

$$\int_0^T J(x,s)\,\frac{\partial u}{\partial s}(x,s)\,ds = -\int_0^T \frac{\partial J}{\partial s}(x,s)u(x,s)ds$$

Compute $\frac{\partial J}{\partial s}(x,s)$:

$$\frac{\partial J}{\partial s}(x,s) = -\alpha(x)\int_s^T (t-s)^{-\alpha(x)-1}u(x,t)\,dt$$

Substitute back:

$$I = \int_\Omega \frac{1}{\Gamma(1-\alpha(x))}\left[-\int_0^T\left(-\alpha(x)\int_s^T (t-s)^{-\alpha(x)-1}u(x,t)dt\right)u(x,s)ds\right]dx$$

$$= \int_\Omega \frac{\alpha(x)}{\Gamma(1-\alpha(x))}\left[\int_0^T\int_s^T (t-s)^{-\alpha(x)-1}u(x,t)u(x,s)\,dt\,ds\right]dx$$

We notice that:

$$|t-s|^{-\alpha(x)-1} = (t-s)^{-\alpha(x)-1} \quad \text{when} \quad t \geq s$$

$$|t-s|^{-\alpha(x)-1} = (s-t)^{-\alpha(x)-1} \quad \text{when} \quad s \geq t$$

Since the function is symmetric, then:

$$\int_0^T\int_0^T |t-s|^{-\alpha(x)-1}u(t)u(s)\,dt\,ds = 2\int_0^T\int_s^T (t-s)^{-\alpha(x)-1}u(t)u(s)\,dt\,ds$$

Symmetrize the double integral:

$$I = \int_\Omega \frac{\alpha(x)}{2\Gamma(1-\alpha(x))}\left[\int_0^T\int_0^T |t-s|^{-\alpha(x)-1}u(x,t)u(x,s)\,dt\,ds\right]dx$$

Sign analysis:

- $\alpha(x) > 0$

- $\Gamma(1-\alpha(x)) > 0$ for $0 < \alpha(x) < 1$
- $|t-s|^{-\alpha(x)-1} \geq 0$ (positive kernel)
- The double integral is a positive quadratic form for $u \in H_0^1$
- Integration over Ω of a nonnegative function yields a nonnegative result

Thus:

$$I \geq 0$$

Hence

$$\int_0^T \left(\partial_t^{\alpha(x)} u(x,t), u(x,t)\right) dt \geq 0$$

3. **Composition rule** : According Riemann-Liouville derivative of variable order

$$\partial_t^{\alpha(x)} u(x,t) = \frac{1}{\Gamma(1-\alpha(x))} \frac{\partial}{\partial t} \int_0^t (t-s)^{-\alpha(x)} u(x,s) ds$$

$$\partial_t^{\beta(x)} u(x,t) = \frac{1}{\Gamma(1-\beta(x))} \frac{\partial}{\partial t} \int_0^t (t-s)^{-\beta(x)} u(x,s)\, ds = v(x,t)$$

$$\partial_t^{\alpha(x)} \partial_t^{\beta(x)} u = \frac{1}{\Gamma(1-\alpha(x))\Gamma(1-\beta(x))} \frac{\partial}{\partial t} \int_0^t (t-s)^{-\alpha(x)} \frac{\partial}{\partial s} \left[\int_0^s (s-\tau)^{-\beta(x)} u(x,\tau)\, d\tau\right] ds$$

Using Leibniz rule: If we have:

$$F(s) = \int_0^s f(s,\tau)\, d\tau$$

then the derivative of $F(s)$ with respect to s is given by:

$$F'(s) = f(s,s) + \int_0^s \frac{\partial}{\partial s} f(s,\tau)\, d\tau$$

where :

$$f(s,\tau) = (s-\tau)^{-\beta(x)} u(x,\tau)$$

$$f(s,s) = (s-s)^{-\beta(x)} u(x,\tau) = 0$$

$$\frac{\partial}{\partial s} f(s,\tau)\,d\tau = \frac{\partial}{\partial s} f(s-\tau)^{-\beta(x)} u(x,\tau) = -\beta(x)(s-\tau)^{-\beta(x)-1} u(x,\tau)\,d\tau$$

we obtain:

$$\frac{\partial}{\partial s}\int_0^s (s-\tau)^{-\beta(x)} u(\tau)\,d\tau = -\beta(x)\int_0^s (s-\tau)^{-\beta(x)-1} u(x,\tau)\,d\tau$$

Therefor

$$\partial_t^{\alpha(x)}\partial_t^{\beta(x)} u(x,t) = -\frac{\beta(x)}{\Gamma(1-\alpha(x))\Gamma(1-\beta(x))}\frac{\partial}{\partial t}\int_0^t (t-s)^{-\alpha(x)}\left[\int_0^s (s-\tau)^{-\beta(x)-1} u(x,\tau)\,d\tau\right] ds$$

Using Fubini's rule:

If we have a double integral over the region $0 \le \tau \le s \le t$:

$$\int_0^t \int_0^s F(s,\tau)\,d\tau\,ds$$

then we can change the order of integration:

$$\int_0^t \int_\tau^t F(s,\tau)\,ds\,d\tau$$

Therefore:

$$\int_0^t \int_0^s F(s,\tau)\,d\tau\,ds = \int_0^t \int_\tau^t F(s,\tau)\,ds\,d\tau$$

$$\partial_t^{\alpha(x)}\partial_t^{\beta(x)} u(x,t) = -\frac{\beta(x)}{\Gamma(1-\alpha(x))\Gamma(1-\beta(x))}\frac{\partial}{\partial t}\int_0^t \int_\tau^t (t-s)^{-\alpha(x)}(s-\tau)^{-\beta(x)-1} u(x,\tau)\,ds\,d\tau$$

Using Beta function:

$$B(p,q) = \int_0^1 t^{p-1}(1-t)^{q-1}\,dt, \quad p>0,\ q>0$$

$$= \frac{\Gamma(p)\Gamma(q)}{\Gamma(p+q)}$$

Then

$$\int_\tau^t (t-s)^{-\alpha}(s-\tau)^{-\beta-1}\,ds = (t-\tau)^{-\alpha-\beta}\cdot B(1-\alpha,-\beta)$$
$$= (t-\tau)^{-\alpha-\beta}\cdot\frac{\Gamma(1-\alpha)\Gamma(-\beta)}{\Gamma(1-\alpha-\beta)}$$

$$\partial_t^{\alpha(x)}\partial_t^{\beta(x)}u(x,t) = -\frac{\beta(x)\Gamma(-\beta(x))}{\Gamma(1-\beta(x))\Gamma(1-\alpha(x)-\beta(x))}\frac{\partial}{\partial t}\int_0^t (t-\tau)^{-\alpha(x)-\beta(x)}u(\tau)\,d\tau$$

Use Gamma identity: $\Gamma(-\beta) = \frac{\Gamma(1-\beta)}{-\beta}$

$$-\frac{\beta\Gamma(-\beta)}{\Gamma(1-\beta)} = 1$$

$$\partial_t^{\alpha(x)}\partial_t^{\beta(x)}u = \frac{1}{\Gamma(1-\alpha(x)-\beta(x))}\frac{\partial}{\partial t}\int_0^t (t-\tau)^{-\alpha(x)-\beta(x)}u(\tau)\,d\tau$$

$$\partial_t^{\alpha(x)}\partial_t^{\beta(x)}u = \frac{1}{\Gamma(1-(\alpha(x)+\beta(x)))}\frac{\partial}{\partial t}\int_0^t (t-\tau)^{-(\alpha(x)+\beta(x))}u(\tau)\,d\tau$$

This is exactly $\partial_t^{\alpha(x)+\beta(x)}u(x,t)$ when α and β depend only on x. Therefore:

$$\partial_t^{\alpha(x)}\partial_t^{\beta(x)}u = \partial_t^{\alpha(x)+\beta(x)}u + R(x,t)$$

with $R(x,t) = 0$ when α and β depend only on x.

■

1.6 Inverse problem formulation and Tikhonov regularization

The objective of this work is to reconstruct the unknown space-dependent fractional order $\alpha(x)$ from observations of the state variable. Let

$$F : \mathcal{A} \longrightarrow L^2(0,T;L^2(\Omega)) \tag{1.7}$$

denote the parameter-to-state map associated with the forward problem, where $F(\alpha) = u(\alpha)$ represents the solution corresponding to a given admissible fractional order α. The inverse problem can then be expressed as

$$F(\alpha) = z^{\delta}, \tag{1.8}$$

where z^{δ} denotes the available observational data.

In practical applications, the measurements are inevitably contaminated by noise arising from experimental errors, numerical approximations, or incomplete observations. Therefore, the available data are assumed to satisfy

$$z^{\delta} = z + \xi, \tag{1.9}$$

where z denotes the exact data, ξ is the noise component, and

$$|\xi|_{L^2(0,T;L^2(\Omega))} \leq \delta, \tag{1.10}$$

with $\delta > 0$ representing the noise level.

As discussed in Section 1.2.2, inverse problems are generally ill-posed in the sense of Hadamard. In particular, small perturbations in the observational data may produce large variations in the reconstructed parameter. Consequently, direct inversion procedures are usually unstable and require additional regularization techniques.

To overcome this difficulty, we employ Tikhonov regularization. The central idea is to replace the original inverse problem by an optimization problem that balances fidelity to the observational data with prior regularity information on the unknown parameter. Similar regularization strategies have been successfully employed for inverse coefficient problems in fractional diffusion equations; see, for example, [15].

The regularized reconstruction problem is formulated as

$$\alpha^* = \arg\min_{\alpha \in \mathcal{A}} J_{\gamma}(\alpha), \tag{1.11}$$

where $\mathcal{A}$ denotes the admissible set and J_{γ} is the Tikhonov functional.

1.6.1 The admissible set

The admissible set contains all fractional orders satisfying the physical and mathematical constraints of the model. Since the fractional order characterizes a subdiffusion process, it must remain strictly between two positive bounds. Furthermore, a certain degree of spatial regularity is required to ensure the well-posedness of the forward problem.

We define

$$\mathcal{A} = \left\{\alpha \in H^1(\Omega) : \alpha_{\min} \leq \alpha(x) \leq \alpha_{\max} \text{ a.e. in } \Omega\right\}, \tag{1.12}$$

where

$$0 < \alpha_{\min} < \alpha_{\max} < 1. \tag{1.13}$$

The admissible set possesses several important properties that play a fundamental role in the variational analysis of the inverse problem:

1. **Convexity.** For any $\alpha_1, \alpha_2 \in \mathcal{A}$ and any $t \in [0,1]$, the convex combination

$$t\alpha_1 + (1-t)\alpha_2 \tag{1.14}$$

also belongs to $\mathcal{A}$.

2. **Closedness in $H^1(\Omega)$.** If a sequence $\{\alpha_n\} \subset \mathcal{A}$ converges strongly in $H^1(\Omega)$ to a function α, then $\alpha \in \mathcal{A}$.

3. **Weak closedness.** The set $\mathcal{A}$ is weakly closed in $H^1(\Omega)$, which guarantees that admissibility is preserved under weak convergence.

4. **Uniform boundedness.** Every admissible parameter satisfies

$$|\alpha|_{L^\infty(\Omega)} \leq \max\{|\alpha_{\min}|, |\alpha_{\max}|\}. \tag{1.15}$$

5. **Lack of boundedness in $H^1(\Omega)$.** Although $\mathcal{A}$ is bounded in $L^\infty(\Omega)$, it is generally not bounded in $H^1(\Omega)$ because the seminorm

$$|\nabla\alpha|_{L^2(\Omega)} \tag{1.16}$$

may become arbitrarily large. This observation motivates the introduction of a regularization term in the optimization functional.

1.6.2 Tikhonov regularization

To stabilize the reconstruction process, we introduce the Tikhonov functional

$$J_\gamma(\alpha) = \frac{1}{2}|F(\alpha) - z^\delta|^2_{L^2(0,T;L^2(\Omega))} + \frac{\gamma}{2}|\nabla\alpha|^2_{L^2(\Omega)}, \tag{1.17}$$

where $\gamma > 0$ is the regularization parameter.

The first term measures the discrepancy between the model prediction and the observational data, while the second term penalizes highly oscillatory reconstructions and promotes stability. Consequently, the minimization problem seeks a compromise between data fitting and regularity of the reconstructed parameter.

The regularization parameter γ controls this balance. Small values of γ emphasize fidelity to the data and may lead to more detailed reconstructions, whereas larger values promote smoother and more stable solutions.

The regularized inverse problem therefore consists of finding

$$\alpha^* = \arg\min_{\alpha\in\mathcal{A}} J_\gamma(\alpha). \tag{1.18}$$

The mathematical analysis of this optimization problem, including the existence of minimizers, stability estimates, and convergence properties of regularized solutions, will be developed in Chapter 3.

1.7 Useful mathematical tools

This section recalls several classical inequalities that will be used throughout the analysis of the forward and inverse problems. These results play an important role in establishing stability estimates, a priori bounds, and convergence properties of the proposed methods.

Theorem 1.7.1 (Young's inequality) *[43] Let $a, b \geq 0$ and let $p, q > 1$ satisfy*

$$\frac{1}{p} + \frac{1}{q} = 1.$$

Then

$$ab \leq \frac{a^p}{p} + \frac{b^q}{q}.$$

Young's inequality is frequently used to estimate products appearing in variational formulations and energy arguments .

Theorem 1.7.2 (Fractional Gronwall inequality) *[9] Let $u : [0,T] \to \mathbb{R}$ be a nonnegative continuous function satisfying*

$$u(t) \le a(t) + b \int_0^t (t-s)^{\gamma-1} u(s)\, ds, \qquad t \in [0,T],$$

where $0 < \gamma < 1$, $b > 0$, and $a(t)$ is a nonnegative nondecreasing continuous function. Then

$$u(t) \le a(t)\, E_\gamma\big(b\,\Gamma(\gamma)\, t^\gamma\big), \qquad t \in [0,T],$$

where

$$E_\gamma(z) = \sum_{k=0}^{\infty} \frac{z^k}{\Gamma(\gamma k + 1)}$$

denotes the Mittag–Leffler function.

The fractional Gronwall inequality is a fundamental tool for deriving stability and continuity estimates in fractional differential equations.

Theorem 1.7.3 (Poincaré inequality) *[5] Let $\Omega \subset \mathbb{R}^d$ be a bounded Lipschitz domain. Then there exists a constant $C_P > 0$ such that*

$$\|u\|_{L^2(\Omega)} \le C_P \|\nabla u\|_{L^2(\Omega)}, \qquad \forall u \in H_0^1(\Omega).$$

The Poincaré inequality provides a fundamental estimate linking the L^2-norm of a function to the norm of its gradient and will be used repeatedly in the variational analysis of the forward problem .

Chapter 2

Analysis of the forward problem

In this chapter, we investigate the well-posedness of the variable-order fractional diffusion problem associated with the space-dependent order $\alpha(x)$. We establish the existence and uniqueness of weak solutions under suitable assumptions on the data and the fractional order. The analysis is based on the Faedo–Galerkin method combined with suitable a priori energy estimates. We also derive additional regularity results and study the continuity of the parameter-to-state map associated with the inverse problem.

2.1 Weak formulation and basic assumptions

We begin by stating the assumptions imposed on the problem data.

Assumption 1 *The following assumptions hold:*

- $u_0 \in H_0^1(\Omega)$,
- $f \in L^2(0,T;L^2(\Omega))$,
- $\alpha \in \mathcal{A}$, *where* $\mathcal{A}$ *is defined in* (1.12).

The weak formulation of problem (1.4) is derived as follows.

Let $v \in H_0^1(\Omega)$ be a test function. Multiplying equation (1.4) by v gives

$$(\partial_t^{\alpha(x)} u)v - (\Delta u)v = fv.$$

Integrating over the spatial domain Ω, we obtain

$$\int_\Omega (\partial_t^{\alpha(x)} u)v \, dx - \int_\Omega (\Delta u)v \, dx = \int_\Omega fv \, dx.$$

Applying Green's identity to the Laplacian term yields

$$-\int_\Omega (\Delta u)v \, dx = \int_\Omega \nabla u \cdot \nabla v \, dx - \int_{\partial\Omega} \frac{\partial u}{\partial n} v \, dS.$$

Since $v \in H_0^1(\Omega)$, we have $v = 0$ on $\partial\Omega$, and therefore the boundary term vanishes. Consequently,

$$-\int_\Omega (\Delta u)v \, dx = \int_\Omega \nabla u \cdot \nabla v \, dx.$$

Substituting this expression into the previous equation gives the weak formulation.

Thus, we seek

$$u(\alpha) \in L^2(0, T; H_0^1(\Omega))$$

such that for all $v \in H_0^1(\Omega)$ and almost every $t \in (0, T]$,

$$(\partial_t^{\alpha(x)} u, v) + (\nabla u, \nabla v) = (f, v). \tag{2.1}$$

The initial condition is given by

$$u(0) = u_0.$$

2.2 Well-posedness

We now establish the well-posedness of the forward problem in the sense of Hadamard (see Definition (1.2.2)).

Theorem 2.2.1 (Existence and uniqueness) *Assume that*

$$u_0 \in H_0^1(\Omega), \qquad f \in L^2(0, T; L^2(\Omega)),$$

and $\alpha \in \mathcal{A}$. Then there exists a unique weak solution

$$u \in L^2(0,T;H_0^1(\Omega)) \cap C([0,T];L^2(\Omega))$$

such that

$$(\partial_t^{\alpha(x)} u(t), v) + (\nabla u(t), \nabla v) = (f(t), v)$$

for all $v \in H_0^1(\Omega)$ and almost every $t \in (0,T]$, together with the initial condition $u(0) = u_0$.

Proof.

1. Existence

We first reduce the problem to one with homogeneous initial data. Define

$$w(x,t) = u(x,t) - u_0(x).$$

Then $w(0) = 0$, $w|_{\partial\Omega} = 0$, and w satisfies

$$(\partial_t^{\alpha(x)} w(t), v) + (\nabla w(t), \nabla v) = \langle G(t), v\rangle, \qquad \forall v \in H_0^1(\Omega), \tag{2.2}$$

where

$$\langle G(t), v\rangle = (f(t), v) - (\nabla u_0, \nabla v).$$

Since

$$f \in L^2(0,T;L^2(\Omega)) \quad \text{and} \quad u_0 \in H_0^1(\Omega),$$

we have

$$G \in L^2(0,T;H^{-1}(\Omega)).$$

Galerkin approximation

Let $\{\varphi_k\}_{k\geq 1} \subset H_0^1(\Omega)$ be an orthonormal basis of $L^2(\Omega)$ and define

$$X_m = \operatorname{span}\{\varphi_1, \ldots, \varphi_m\}.$$

We seek an approximate solution of the form

$$w_m(t) = \sum_{j=1}^{m} c_j^{(m)}(t)\varphi_j, \qquad c_j^{(m)}(0) = 0,$$

satisfying

$$(\partial_t^{\alpha(x)} w_m(t), v) + (\nabla w_m(t), \nabla v) = \langle G(t), v \rangle, \qquad \forall v \in X_m. \tag{2.3}$$

Since X_m is finite-dimensional, problem (2.3) reduces to a finite system of linear Volterra integral equations for the coefficients $c_j^{(m)}(t)$. Since $0 < \alpha(x) < 1$, the kernel associated with the Caputo derivative is integrable over finite time intervals. Therefore, standard Volterra theory ensures the existence and uniqueness of $w_m \in C([0,T]; X_m)$.

Energy estimate

Choosing $v = w_m(t)$ in (2.3), we obtain

$$(\partial_t^{\alpha(x)} w_m(t), w_m(t)) + \|\nabla w_m(t)\|^2_{L^2(\Omega)} = \langle G(t), w_m(t) \rangle.$$

Integrating over $(0,T)$ yields

$$\int_0^T (\partial_t^{\alpha(x)} w_m, w_m)\, dt + \int_0^T \|\nabla w_m\|^2_{L^2(\Omega)}\, dt = \int_0^T \langle G, w_m \rangle\, dt.$$

Since $w_m(0) = 0$ and $0 < \alpha(x) < 1$, the Caputo term is nonnegative:

$$\int_0^T (\partial_t^{\alpha(x)} w_m, w_m)\, dt \geq 0.$$

Hence,

$$\int_0^T \|\nabla w_m\|^2_{L^2(\Omega)}\, dt \leq \int_0^T \langle G, w_m \rangle\, dt.$$

Using the duality pairing together with Young's inequality, we obtain

$$\|\nabla w_m\|^2_{L^2(0,T;L^2(\Omega))} \leq C \|G\|^2_{L^2(0,T;H^{-1}(\Omega))}.$$

Hence, the sequence $\{w_m\}$ is uniformly bounded in $L^2(0,T; H_0^1(\Omega))$.

Passage to the limit

Since $L^2(0,T; H_0^1(\Omega))$ is a Hilbert space, there exist a subsequence, still denoted by $\{w_m\}$, and a function $w \in L^2(0,T; H_0^1(\Omega))$ such that

$$w_m \rightharpoonup w \quad \text{weakly in } L^2(0,T; H_0^1(\Omega)).$$

In particular,

$$\nabla w_m \rightharpoonup \nabla w \quad \text{weakly in } L^2(0,T;L^2(\Omega)).$$

From (2.3), we may write

$$\partial_t^{\alpha(x)} w_m = G - (-\Delta w_m),$$

which implies that $\partial_t^{\alpha(x)} w_m$ is bounded in $L^2(0,T;H^{-1}(\Omega))$. Therefore, there exists $\eta \in L^2(0,T;H^{-1}(\Omega))$ such that, up to a subsequence,

$$\partial_t^{\alpha(x)} w_m \rightharpoonup \eta \quad \text{weakly in } L^2(0,T;H^{-1}(\Omega)).$$

Let $v \in H_0^1(\Omega)$. Since X_m is dense in $H_0^1(\Omega)$, there exists $v_m \in X_m$ such that

$$v_m \to v \quad \text{strongly in } H_0^1(\Omega).$$

Passing to the limit in the Galerkin formulation gives

$$\langle \eta(t), v\rangle + (\nabla w(t), \nabla v) = \langle G(t), v\rangle, \qquad \forall v \in H_0^1(\Omega),$$

for almost every $t \in (0,T)$. By weak sequential closedness of the Caputo operator, we identify $\eta = \partial_t^{\alpha(x)} w$. Consequently, w satisfies (2.2). Finally, defining $u = w + u_0$, we conclude that u is a weak solution of the original problem.

2. Continuity in time

We next establish the temporal continuity of the weak solution.

From the estimates obtained above,

$$w \in L^2(0,T;H_0^1(\Omega)), \qquad \partial_t^{\alpha(x)} w \in L^2(0,T;H^{-1}(\Omega)).$$

Standard compactness and energy arguments for fractional evolution equations imply that $w \in C([0,T];L^2(\Omega))$. We refer, for example, to [18] for the corresponding argument in the constant-order case; the same reasoning applies here since the fractional order depends only on the spatial variable. Since $u = w + u_0$ and $u_0 \in L^2(\Omega)$, it follows that $u \in C([0,T];L^2(\Omega))$.

3. Uniqueness

Let u_1 and u_2 be two weak solutions and define $\phi = u_1 - u_2$. Then $\phi(0) = 0$ and

$$(\partial_t^{\alpha(x)}\phi, v) + (\nabla\phi, \nabla v) = 0, \qquad \forall v \in H_0^1(\Omega).$$

Choosing $v = \phi(t)$ and integrating over $(0, T)$, we obtain

$$\int_0^T (\partial_t^{\alpha(x)}\phi, \phi)\, dt + \int_0^T \|\nabla\phi\|_{L^2(\Omega)}^2\, dt = 0.$$

Both terms are nonnegative, and therefore both must vanish. Consequently,

$$\nabla\phi = 0 \quad \text{a.e. in } \Omega \times (0, T).$$

Since $\phi \in H_0^1(\Omega)$, we conclude that $\phi = 0$, which implies $u_1 = u_2$. This completes the proof.

■

2.3 Enhanced regularity

We now establish additional regularity properties of the weak solution under stronger assumptions on the initial data, source term, and fractional order. These estimates play an important role in the convergence analysis and numerical approximation developed in the subsequent chapters.

Assumption 2 *Assume that the following conditions are satisfied:*

- *The domain $\Omega \subset \mathbb{R}^d$ is bounded with Lipschitz boundary $\partial\Omega$.*
- *The variable-order function satisfies*

$$\alpha \in C(\overline{\Omega}), \qquad 0 < \alpha_{\min} \le \alpha(x) \le \alpha_{\max} < 1, \quad \forall x \in \overline{\Omega}.$$

- *The source term satisfies*

$$f \in L^2(0, T; L^2(\Omega)).$$

- *The initial data satisfies* $u_0 \in H_0^1(\Omega)$.

Remark 2.3.1 *The second assumption is essential for the analysis of the variable-order Caputo derivative, since it guarantees that the fractional order remains strictly between* 0 *and* 1*, thereby excluding degenerate or singular cases.*

Theorem 2.3.2 (Enhanced regularity) *Assume additionally that*

- $u_0 \in \widetilde{H}^2(\Omega)$,
- $f \in C^1([0,T]; L^2(\Omega))$,
- $\alpha \in W^{1,\infty}(\Omega)$.

Then, for every $t \in (0,T]$*, the weak solution satisfies*

$$\|u(t)\|_{\widetilde{H}^2(\Omega)} + t^{1-\alpha_{\min}} \|\partial_t u(t)\|_{L^2(\Omega)} \leq C,$$

where the constant C *depends on*

$$\|u_0\|_{\widetilde{H}^2(\Omega)}, \qquad \|f\|_{C^1([0,T];L^2(\Omega))}, \text{ and } \|\alpha\|_{W^{1,\infty}(\Omega)}.$$

Proof.

Let $A = -\Delta$ denote the Dirichlet Laplacian with domain $D(A) = \widetilde{H}^2(\Omega)$. Let $\{\varphi_k\}_{k\geq 1}$ be the eigenfunctions of A and define

$$X_m = \operatorname{span}\{\varphi_1, \ldots, \varphi_m\}.$$

We consider the Galerkin approximation $u_m(t) \in X_m$ satisfying

$$(\partial_t^{\alpha(x)} u_m(t), v) + (Au_m(t), v) = (f(t), v), \qquad \forall v \in X_m,$$

with $u_m(0) = P_m u_0$, where P_m denotes the $L^2(\Omega)$ projection onto X_m. Since $Au_m(t) \in X_m$, we may choose $v = Au_m(t)$. Consequently,

$$(\partial_t^{\alpha(x)} u_m(t), Au_m(t)) + \|Au_m(t)\|_{L^2(\Omega)}^2 = (f(t), Au_m(t)). \tag{2.4}$$

Since the fractional order depends on the spatial variable, spatial differentiation does not commute with the variable-order Caputo operator. More precisely,

$$\nabla(\partial_t^{\alpha(x)} u_m) = \partial_t^{\alpha(x)}(\nabla u_m) + R_m,$$

where the commutator term satisfies

$$\|R_m(t)\|_{L^2(\Omega)} \le C\|\nabla\alpha\|_{L^\infty(\Omega)} \int_0^t (t-s)^{-\alpha_{\min}} \big(1 + |\log(t-s)|\big) \|u_{m,t}(s)\|_{L^2(\Omega)}\, ds. \tag{2.5}$$

This estimate follows from differentiating the kernel $(t-s)^{-\alpha(x)}$ with respect to the spatial variable and using the boundedness of $\nabla\alpha$ together with the smoothness of the Gamma function.

Using integration by parts, we obtain

$$(\partial_t^{\alpha(x)} u_m, Au_m) = (\nabla(\partial_t^{\alpha(x)} u_m), \nabla u_m).$$

Hence,

$$(\partial_t^{\alpha(x)} u_m, Au_m) = (\partial_t^{\alpha(x)} \nabla u_m, \nabla u_m) + (R_m, \nabla u_m).$$

Integrating (2.4) over $(0,t)$ and using Young's inequality gives

$$\int_0^t \|Au_m(s)\|_{L^2(\Omega)}^2\, ds \le C\|u_0\|_{\widetilde{H}^2(\Omega)}^2 + C\int_0^t \|f(s)\|_{L^2(\Omega)}^2\, ds + C\int_0^t \|R_m(s)\|_{L^2(\Omega)}^2\, ds.$$

Using the commutator estimate together with Young's inequality for convolutions yields

$$\int_0^t \|R_m(s)\|_{L^2(\Omega)}^2\, ds \le C\|\alpha\|_{W^{1,\infty}(\Omega)}^2 \int_0^t \left(\int_0^s (s-\tau)^{-\alpha_{\min}} \|u_{m,t}(\tau)\|_{L^2(\Omega)}\, d\tau \right)^2 ds.$$

Since the Galerkin system is finite-dimensional and

$$f \in C^1([0,T]; L^2(\Omega)),$$

differentiation with respect to time is justified. Differentiating the Galerkin equation yields

$$\partial_t(\partial_t^{\alpha(x)} u_m) + Au_{m,t} = f_t.$$

Testing this equation with $u_{m,t}$ and using the standard fractional energy method for subdiffusion equations (see [37]), we obtain

$$t^{1-\alpha_{\min}}\|u_{m,t}(t)\|_{L^2(\Omega)} \leq C\left(\|u_0\|_{\tilde{H}^2(\Omega)} + \|f\|_{C^1([0,T];L^2(\Omega))}\right).$$

Using the representation formula for the Caputo derivative together with the previous estimate gives

$$\|\partial_t^{\alpha(x)} u_m(t)\|_{L^2(\Omega)} \leq C.$$

Since

$$Au_m(t) = f(t) - \partial_t^{\alpha(x)} u_m(t),$$

we conclude that

$$\|Au_m(t)\|_{L^2(\Omega)} \leq C.$$

Finally, elliptic regularity implies

$$\|u_m(t)\|_{\tilde{H}^2(\Omega)} \leq C\|Au_m(t)\|_{L^2(\Omega)}.$$

Passing to the limit as $m \to \infty$ yields

$$\|u(t)\|_{\tilde{H}^2(\Omega)} + t^{1-\alpha_{\min}}\|\partial_t u(t)\|_{L^2(\Omega)} \leq C.$$

This completes the proof. ■

2.4 Continuity of the parameter-to-state map

We now study the dependence of the weak solution on the fractional-order parameter $\alpha(x)$.

Definition 2.4.1 (Parameter-to-state map) *Let $\mathcal{A} \subset H^1(\Omega)$ be the admissible set defined in (1.12). For each $\alpha \in \mathcal{A}$, let $u(\alpha)$ denote the unique weak solution of problem (2.1). The parameter-to-state map*

$$F : \mathcal{A} \longrightarrow L^2(0,T;H_0^1(\Omega))$$

is defined by

$$F(\alpha) = u(\alpha).$$

Theorem 2.4.2 (Continuity of the parameter-to-state map) *Assume that*

$$u_0 \in \widetilde{H}^2(\Omega), \qquad f \in C^1([0,T]; L^2(\Omega)).$$

Let $\alpha_n, \alpha \in \mathcal{A}$ *such that* $\alpha_n \to \alpha$ *in* $H^1(\Omega)$. *Denote by* $u_n = u(\alpha_n)$, $u = u(\alpha)$ *the corresponding weak solutions of the forward problem. Then*

$$u_n \to u \quad \text{in } L^2(0,T; H_0^1(\Omega)).$$

In particular, the parameter-to-state map

$$F : \mathcal{A} \to L^2(0,T; H_0^1(\Omega))$$

is continuous.

Proof.

Define $w_n = u_n - u$. Subtracting the weak formulations satisfied by u_n and u, we obtain

$$(\partial_t^{\alpha_n(x)} u_n - \partial_t^{\alpha(x)} u, v) + (\nabla w_n, \nabla v) = 0,$$

for all $v \in H_0^1(\Omega)$. We decompose the fractional term as follows:

$$\partial_t^{\alpha_n(x)} u_n - \partial_t^{\alpha(x)} u = \partial_t^{\alpha_n(x)} w_n + r_n,$$

where $r_n = \partial_t^{\alpha_n(x)} u - \partial_t^{\alpha(x)} u$. Therefore,

$$(\partial_t^{\alpha_n(x)} w_n, v) + (\nabla w_n, \nabla v) = -(r_n, v).$$

Since the initial data are identical, $w_n(0) = 0$. Choosing $v = w_n(t)$ and integrating over $(0,T)$ yields

$$\int_0^T (\partial_t^{\alpha_n(x)} w_n, w_n)\, dt + \int_0^T \|\nabla w_n\|^2_{L^2(\Omega)}\, dt = -\int_0^T (r_n, w_n)\, dt.$$

By the positivity property of the Caputo derivative, the first term is nonnegative. Hence,

$$\int_0^T \|\nabla w_n\|^2_{L^2(\Omega)}\, dt \le \left| \int_0^T (r_n, w_n)\, dt \right|.$$

Using the duality pairing between

$$H^{-1}(\Omega) \quad \text{and} \quad H_0^1(\Omega),$$

together with Young's inequality, we obtain

$$\|\nabla w_n\|_{L^2(0,T;L^2(\Omega))} \leq C\|r_n\|_{L^2(0,T;H^{-1}(\Omega))}.$$

It therefore remains to prove that

$$\|r_n\|_{L^2(0,T;H^{-1}(\Omega))} \to 0.$$

Using the representation formula for the variable-order Caputo derivative,

$$\partial_t^{\beta(x)} u(x,t) = \frac{1}{\Gamma(1-\beta(x))} \int_0^t (t-s)^{-\beta(x)} u_t(x,s)\, ds,$$

and applying the mean value theorem with respect to the parameter β, we obtain

$$r_n(x,t) = (\alpha_n(x) - \alpha(x)) G'(\alpha_\theta(x)),$$

where

$$\alpha_\theta(x) = \alpha(x) + \theta(x)(\alpha_n(x) - \alpha(x)),$$

with $0 < \theta(x) < 1$. Differentiation of the kernel with respect to the order parameter yields

$$|G'(\beta)| \leq C \int_0^t (t-s)^{-\alpha_{\min}} (1 + |\log(t-s)|) |u_t(x,s)|\, ds.$$

Since $\alpha_n \to \alpha \quad \text{in } H^1(\Omega)$, we also have

$$\alpha_n \to \alpha \quad \text{in } L^2(\Omega).$$

Therefore,

$$\|r_n(t)\|_{H^{-1}(\Omega)} \leq C\|\alpha_n - \alpha\|_{L^2(\Omega)} \left\| \int_0^t (t-s)^{-\alpha_{\min}} (1 + |\log(t-s)|) |u_t(\cdot,s)|\, ds \right\|_{L^2(\Omega)}.$$

Define the kernel

$$k(t-s) = (t-s)^{-\alpha_{\min}} (1 + |\log(t-s)|).$$

Since $0 < \alpha_{\min} < 1$, we have $k \in L^1(0,T)$. Using Young's convolution inequality together with the regularity

$$u_t \in L^2(0,T;L^2(\Omega)),$$

we obtain

$$\|r_n\|_{L^2(0,T;H^{-1}(\Omega))} \leq C\|\alpha_n - \alpha\|_{L^2(\Omega)}.$$

Consequently,

$$\|r_n\|_{L^2(0,T;H^{-1}(\Omega))} \to 0.$$

Hence,

$$\|\nabla w_n\|_{L^2(0,T;L^2(\Omega))} \to 0,$$

which implies

$$u_n \to u \quad \text{in } L^2(0,T;H_0^1(\Omega)).$$

Therefore, the parameter-to-state map is continuous.

■

Theorem 2.4.3 (Fréchet differentiability) *The parameter-to-state map*

$$F : A \to L^2(0,T;H_0^1(\Omega)), \qquad F(\alpha) = u(\alpha),$$

is Fréchet differentiable. For $\alpha, h \in A$ with $\alpha + h \in A$, the derivative $v = F'(\alpha)h$ is characterized as the unique solution of

$$\partial_t^{\alpha(x)} v - \Delta v = -\left(\frac{\partial}{\partial \alpha}\partial_t^{\alpha(x)} u(\alpha)\right) h,$$

with homogeneous initial and boundary conditions, where

$$\frac{\partial}{\partial \alpha}\left(\partial_t^{\alpha(x)} w\right) = -\psi(1-\alpha(x))\,\partial_t^{\alpha(x)} w + \frac{1}{\Gamma(1-\alpha(x))}\int_0^t (t-s)^{-\alpha(x)} \log(t-s)\,\partial_s w(x,s)\,ds.$$

Proof. Let $\alpha \in A$ be fixed and let $h \in H^1(\Omega)$ be such that $\alpha + h \in A$. Denote by $u = u(\alpha)$ and $u_h = u(\alpha + h)$ the corresponding weak solutions of the forward problem. We aim to show that the map $F : \alpha \mapsto u(\alpha)$ is Fréchet differentiable at α, and to identify its derivative.

By definition, u and u_h satisfy

$$\partial_t^{\alpha(x)} u - \Delta u = f, \qquad \partial_t^{\alpha(x)+h(x)} u_h - \Delta u_h = f,$$

with identical initial and boundary conditions. Subtracting the two equations yields

$$\partial_t^{\alpha(x)}(u_h - u) - \Delta(u_h - u) = -\left(\partial_t^{\alpha(x)+h(x)} u_h - \partial_t^{\alpha(x)} u_h\right).$$

We now expand the fractional operator with respect to the order. For each sufficiently regular function w, define

$$G(\beta) := \partial_t^{\beta(x)} w.$$

Using the integral definition of the variable-order Caputo derivative and differentiation under the integral sign, one verifies that G is Fréchet differentiable with respect to β, and that its derivative at $\beta = \alpha$ is given by

$$\frac{\partial}{\partial \alpha}\left(\partial_t^{\alpha(x)} w\right) = -\psi(1-\alpha(x))\,\partial_t^{\alpha(x)} w + \frac{1}{\Gamma(1-\alpha(x))}\int_0^t (t-s)^{-\alpha(x)} \log(t-s)\,\partial_s w(x,s)\,ds.$$

Moreover, there exists a constant C such that for all sufficiently small h,

$$\left\| \partial_t^{\alpha+h} w - \partial_t^{\alpha} w - \left(\frac{\partial}{\partial \alpha}\partial_t^{\alpha} w\right) h \right\| \leq C \|h\|^2_{L^\infty(\Omega)}.$$

Applying this expansion with $w = u_h$, we obtain

$$\partial_t^{\alpha+h} u_h - \partial_t^{\alpha} u_h = \left(\frac{\partial}{\partial \alpha}\partial_t^{\alpha} u_h\right) h + R_h,$$

where $\|R_h\| \leq C\|h\|^2$.

Motivated by this expansion, we define $v = F'(\alpha)h$ as the solution of the linearized problem

$$\partial_t^{\alpha(x)} v - \Delta v = -\left(\frac{\partial}{\partial \alpha}\partial_t^{\alpha(x)} u\right) h,$$

with homogeneous initial and boundary conditions. By linearity of the forward operator in the state variable, v depends linearly on h.

Define the remainder

$$r_h := u_h - u - v.$$

Subtracting the equations for u_h, u, and v, we find that r_h satisfies

$$\partial_t^{\alpha(x)} r_h - \Delta r_h = -\left(\partial_t^{\alpha+h} u_h - \partial_t^{\alpha} u_h - \left(\frac{\partial}{\partial \alpha}\partial_t^{\alpha} u\right) h\right).$$

Adding and subtracting $\left(\frac{\partial}{\partial \alpha}\partial_t^{\alpha} u_h\right) h$, we rewrite the right-hand side as

$$-\left(\partial_t^{\alpha+h} u_h - \partial_t^{\alpha} u_h - \left(\frac{\partial}{\partial \alpha}\partial_t^{\alpha} u_h\right) h\right) - \left(\left(\frac{\partial}{\partial \alpha}\partial_t^{\alpha} u_h\right) - \left(\frac{\partial}{\partial \alpha}\partial_t^{\alpha} u\right)\right) h.$$

The first term is of order $O(\|h\|^2)$ by the Taylor estimate. For the second term, using linearity and boundedness of the derivative operator together with continuity of the parameter-to-state map, we have

$$\|u_h - u\| \leq C\|h\|,$$

which implies that this term is also of order $O(\|h\|^2)$. Therefore,

$$\|\text{RHS}\| \leq C\|h\|^2.$$

By stability estimates for the forward problem with fixed α, it follows that

$$\|r_h\| \leq C\|h\|^2.$$

Consequently,

$$\frac{\|u_h - u - v\|}{\|h\|} \leq C\|h\| \to 0 \quad \text{as } \|h\| \to 0.$$

This proves that F is Fréchet differentiable at α, with derivative $F'(\alpha)h = v$, where v is the unique solution of the linearized problem. This completes the proof. ■

Chapter 3

Inverse Problem and Numerical Approximation

In this chapter, we investigate the inverse problem of recovering the space-dependent fractional order $\alpha(x)$ from noisy observations z^δ. Since the problem is inherently ill-posed, we employ Tikhonov regularization in order to obtain a stable reconstruction framework. The resulting optimization problem is analyzed theoretically and then discretized numerically.

To approximate the forward problem, we combine finite element discretization in space with convolution quadrature in time. Furthermore, the Fréchet differentiability of the parameter-to-state map allows the computation of gradients required for optimization algorithms. Finally, we formulate the fully discrete inverse problem and study the convergence properties of discrete minimizers.

3.1 Existence of minimizers

We establish the existence of minimizers for the regularized inverse problem. The proof is based on the direct method of the calculus of variations together with the continuity

properties of the parameter-to-state map established in Chapter 2.

Theorem 3.1.1 (Existence of minimizers) *Let $z^\delta \in L^2(0,T;L^2(\Omega))$ and let $\gamma > 0$. Then the minimization problem $\min_{\alpha\in\mathcal{A}} J_\gamma(\alpha)$ admits at least one minimizer $\alpha^* \in \mathcal{A}$.*

Proof. Let $j_* = \inf_{\alpha\in A} J_\gamma(\alpha)$. By definition of the infimum, there exists a minimizing sequence $\{\alpha_n\} \subset A$ such that

$$J_\gamma(\alpha_n) \to j_* \quad \text{as } n \to \infty.$$

Since this sequence converges, it is bounded. Hence there exists a constant $C > 0$ such that $J_\gamma(\alpha_n) \le C$. From the definition of J_γ we obtain

$$\frac{\gamma}{2}\|\nabla\alpha_n\|^2_{L^2(\Omega)} \le J_\gamma(\alpha_n) \le C,$$

which implies that the sequence $\{\nabla\alpha_n\}$ is bounded in $L^2(\Omega)$. Moreover, the box constraints defining the admissible set A yield

$$\alpha_{\min} \le \alpha_n(x) \le \alpha_{\max} \quad \text{a.e. in } \Omega,$$

and therefore $\{\alpha_n\}$ is bounded in $L^2(\Omega)$. Combining these estimates shows that $\{\alpha_n\}$ is bounded in $H^1(\Omega)$.

Since $H^1(\Omega)$ is reflexive, there exists a subsequence (still denoted by $\{\alpha_n\}$) and a function $\alpha^* \in H^1(\Omega)$ such that

$$\alpha_n \rightharpoonup \alpha^* \quad \text{weakly in } H^1(\Omega).$$

Furthermore, the compact embedding $H^1(\Omega) \hookrightarrow L^2(\Omega)$ implies that

$$\alpha_n \to \alpha^* \quad \text{strongly in } L^2(\Omega).$$

Consequently, after extraction of a further subsequence if necessary,

$$\alpha_n(x) \to \alpha^*(x) \quad \text{a.e. in } \Omega.$$

Since each α_n satisfies the bounds $\alpha_{\min} \le \alpha_n(x) \le \alpha_{\max}$, passing to the limit yields

$$\alpha_{\min} \le \alpha^*(x) \le \alpha_{\max} \quad \text{a.e. in } \Omega,$$

and therefore $\alpha^* \in A$.

The regularization term is weakly lower semicontinuous in $H^1(\Omega)$, which gives

$$\|\nabla\alpha^*\|^2_{L^2(\Omega)} \leq \liminf_{n\to\infty} \|\nabla\alpha_n\|^2_{L^2(\Omega)}.$$

Moreover, the parameter-to-state map

$$F(\alpha) = u(\alpha)$$

is continuous from $L^2(\Omega)$ to $L^2(0,T;L^2(\Omega))$. Hence the convergence $\alpha_n \to \alpha^*$ in $L^2(\Omega)$ implies

$$u(\alpha_n) \to u(\alpha^*) \quad \text{in } L^2(0,T;L^2(\Omega)).$$

Consequently,

$$\|u(\alpha_n) - z^\delta\|_{L^2(0,T;L^2(\Omega))} \to \|u(\alpha^*) - z^\delta\|_{L^2(0,T;L^2(\Omega))}.$$

Combining the previous estimates yields

$$J_\gamma(\alpha^*) \leq \liminf_{n\to\infty} J_\gamma(\alpha_n) = j_*.$$

Since j_* is the infimum of J_γ over A, we also have $J_\gamma(\alpha^*) \geq j_*$. Therefore $J_\gamma(\alpha^*) = j_*$, which proves that α^* is a minimizer of the functional J_γ over the admissible set A.

■

3.1.1 Stability under noise

An important aspect of regularization methods is their stability with respect to perturbations in the observational data. In practical applications, measurements are always contaminated by noise, and therefore it is essential to guarantee that the reconstructed parameters depend continuously on the data.

In this section, we analyze the behavior of Tikhonov minimizers when the noise level tends to zero. Under suitable assumptions on the regularization parameter, we show that the regularized solutions converge to an exact solution of the inverse problem with minimal H^1-seminorm.

Theorem 3.1.2 (Stability of Tikhonov minimizers) *Let $\{\delta_n\} \subset \mathbb{R}_+$ be such that $\delta_n \to 0$, and let $\{z^{\delta_n}\} \subset L^2(0,T;L^2(\Omega))$ be noisy observations satisfying*

$$\|z^{\delta_n} - u(\alpha^\dagger)\|_{L^2(0,T;L^2(\Omega))} \leq \delta_n,$$

where $\alpha^\dagger \in \mathcal{A}$ is an exact solution of the inverse problem.

Assume that the regularization parameters $\{\gamma_n\} \subset \mathbb{R}_+$ satisfy

$$\gamma_n \to 0, \qquad \frac{\delta_n^2}{\gamma_n} \to 0.$$

For each $n \in \mathbb{N}$, let $\alpha_n^* \in \mathcal{A}$ be a minimizer of the Tikhonov functional $J_{\gamma_n}(\cdot; z^{\delta_n})$ over $\mathcal{A}$. Then the sequence $\{\alpha_n^*\}$ contains a subsequence converging strongly in $H^1(\Omega)$ to a minimum-H^1-seminorm solution $\bar{\alpha}$ of the inverse problem.

Proof. For each $n \in \mathbb{N}$, define

$$J_n(\alpha) = \frac{1}{2}\|u(\alpha) - z^{\delta_n}\|^2_{L^2(0,T;L^2(\Omega))} + \frac{\gamma_n}{2}\|\nabla\alpha\|^2_{L^2(\Omega)}, \qquad \alpha \in \mathcal{A}.$$

Since α_n^* minimizes J_n over $\mathcal{A}$, we have

$$J_n(\alpha_n^*) \leq J_n(\alpha^\dagger).$$

Using the noise estimate and the identity $u(\alpha^\dagger)$ for the exact data, this gives

$$\frac{1}{2}\|u(\alpha_n^*) - z^{\delta_n}\|^2_{L^2(0,T;L^2(\Omega))} + \frac{\gamma_n}{2}\|\nabla\alpha_n^*\|^2_{L^2(\Omega)} \leq \frac{1}{2}\delta_n^2 + \frac{\gamma_n}{2}\|\nabla\alpha^\dagger\|^2_{L^2(\Omega)}.$$

Hence,

$$\|u(\alpha_n^*) - z^{\delta_n}\|^2_{L^2(0,T;L^2(\Omega))} + \gamma_n\|\nabla\alpha_n^*\|^2_{L^2(\Omega)} \leq \delta_n^2 + \gamma_n\|\nabla\alpha^\dagger\|^2_{L^2(\Omega)}.$$

Dividing by γ_n yields

$$\|\nabla\alpha_n^*\|^2_{L^2(\Omega)} \leq \frac{\delta_n^2}{\gamma_n} + \|\nabla\alpha^\dagger\|^2_{L^2(\Omega)}.$$

Since $\delta_n^2/\gamma_n \to 0$, the sequence $\{\nabla\alpha_n^*\}$ is bounded in $L^2(\Omega)$. Together with the box constraints defining $\mathcal{A}$, this implies that $\{\alpha_n^*\}$ is bounded in $H^1(\Omega)$.

Therefore, by the reflexivity of $H^1(\Omega)$, there exist a subsequence, still denoted by $\{\alpha_n^*\}$, and a function $\bar{\alpha} \in H^1(\Omega)$ such that

$$\alpha_n^* \rightharpoonup \bar{\alpha} \quad \text{weakly in } H^1(\Omega).$$

Moreover, since the embedding $H^1(\Omega) \hookrightarrow L^2(\Omega)$ is compact, we also have

$$\alpha_n^* \to \bar{\alpha} \quad \text{strongly in } L^2(\Omega).$$

Because the admissible set $\mathcal{A}$ is weakly closed in $H^1(\Omega)$, it follows that $\bar{\alpha} \in \mathcal{A}$.

From the previous estimate, we also obtain

$$\|u(\alpha_n^*) - z^{\delta_n}\|_{L^2(0,T;L^2(\Omega))} \to 0.$$

Using the triangle inequality, we get

$$\|u(\alpha_n^*) - u(\alpha^\dagger)\|_{L^2(0,T;L^2(\Omega))} \leq \|u(\alpha_n^*) - z^{\delta_n}\|_{L^2(0,T;L^2(\Omega))} + \|z^{\delta_n} - u(\alpha^\dagger)\|_{L^2(0,T;L^2(\Omega))}.$$

Since both terms on the right-hand side tend to zero, we conclude that

$$u(\alpha_n^*) \to u(\alpha^\dagger) \quad \text{strongly in } L^2(0,T;L^2(\Omega)).$$

By the sequential closedness of the parameter-to-state map, the convergences

$$\alpha_n^* \to \bar{\alpha} \quad \text{in } L^2(\Omega), \qquad u(\alpha_n^*) \to u(\alpha^\dagger) \quad \text{in } L^2(0,T;L^2(\Omega))$$

imply $u(\bar{\alpha}) = u(\alpha^\dagger)$. Thus, $\bar{\alpha}$ is an exact solution of the inverse problem.

It remains to show that $\bar{\alpha}$ has minimum H^1-seminorm among all exact solutions. Let $\widetilde{\alpha} \in \mathcal{A}$ be any exact solution, that is, $u(\widetilde{\alpha}) = u(\alpha^\dagger)$. By the minimality of α_n^*, we have

$$J_n(\alpha_n^*) \leq J_n(\widetilde{\alpha}).$$

Since $\widetilde{\alpha}$ is an exact solution, the noise estimate gives

$$\|u(\widetilde{\alpha}) - z^{\delta_n}\|_{L^2(0,T;L^2(\Omega))} = \|u(\alpha^\dagger) - z^{\delta_n}\|_{L^2(0,T;L^2(\Omega))} \leq \delta_n.$$

Consequently,

$$\|\nabla \alpha_n^*\|_{L^2(\Omega)}^2 \leq \frac{\delta_n^2}{\gamma_n} + \|\nabla \widetilde{\alpha}\|_{L^2(\Omega)}^2.$$

Passing to the limit superior, and using $\delta_n^2/\gamma_n \to 0$, yields

$$\limsup_{n\to\infty} \|\nabla \alpha_n^*\|_{L^2(\Omega)}^2 \leq \|\nabla \widetilde{\alpha}\|_{L^2(\Omega)}^2.$$

On the other hand, weak lower semicontinuity gives

$$\|\nabla\bar{\alpha}\|^2_{L^2(\Omega)} \leq \liminf_{n\to\infty} \|\nabla\alpha_n^*\|^2_{L^2(\Omega)}.$$

Combining the two inequalities, we obtain

$$\|\nabla\bar{\alpha}\|^2_{L^2(\Omega)} \leq \|\nabla\widetilde{\alpha}\|^2_{L^2(\Omega)}.$$

Since $\widetilde{\alpha}$ was arbitrary, $\bar{\alpha}$ is a minimum-H^1-seminorm solution.

Finally, choosing $\widetilde{\alpha} = \bar{\alpha}$ in the previous estimate gives

$$\limsup_{n\to\infty} \|\nabla\alpha_n^*\|^2_{L^2(\Omega)} \leq \|\nabla\bar{\alpha}\|^2_{L^2(\Omega)}.$$

Together with weak lower semicontinuity, this implies

$$\|\nabla\alpha_n^*\|_{L^2(\Omega)} \to \|\nabla\bar{\alpha}\|_{L^2(\Omega)}.$$

Since $\alpha_n^* \rightharpoonup \bar{\alpha}$ weakly in $H^1(\Omega)$ and the corresponding seminorms converge, we conclude that

$$\alpha_n^* \to \bar{\alpha} \quad \text{strongly in } H^1(\Omega).$$

The proof is complete. ∎

3.2 Finite element discretization

We now turn to the numerical approximation of the forward problem. In order to compute approximate solutions efficiently, the problem is discretized both in space and in time, leading to a fully discrete scheme suitable for numerical implementation.

The spatial discretization is based on the finite element method, while the temporal discretization relies on convolution quadrature techniques adapted to fractional evolution equations. This combination provides a robust framework capable of accurately capturing both the spatial variability of the solution and the memory effects induced by the fractional derivative.

3.2.1 Spatial discretization

We begin by discretizing the spatial domain using the finite element method. Let $\mathcal{T}_h$ be a shape-regular and quasi-uniform triangulation of the bounded domain $\Omega \subset \mathbb{R}^d$, where

$$h = \max_{T \in \mathcal{T}_h} \operatorname{diam}(T)$$

denotes the mesh size. The Sobolev space $H_0^1(\Omega)$ is approximated by the conforming finite element space

$$X_h = \left\{ v_h \in H^1(\Omega) : v_h|_T \in P_1(T), \quad \forall T \in \mathcal{T}_h \right\} \cap H_0^1(\Omega),$$

where $P_1(T)$ denotes the space of polynomials of degree at most one on the element T. The choice of continuous piecewise linear finite elements guarantees continuity across element interfaces and provides an efficient approximation framework for second-order elliptic operators. Similarly, the unknown fractional-order parameter is approximated in the finite-dimensional space

$$V_h = \left\{ \alpha_h \in H^1(\Omega) : \alpha_h|_T \in P_1(T), \quad \alpha_{\min} \leq \alpha_h(x) \leq \alpha_{\max} \text{ a.e. in } \Omega \right\}.$$

To project functions onto the finite element space, we introduce the L^2-projection operator

$$P_h : L^2(\Omega) \to X_h,$$

defined by

$$(P_h\phi, \chi_h) = (\phi, \chi_h), \qquad \forall \chi_h \in X_h.$$

The operator P_h satisfies the classical approximation estimate

$$\|P_h\phi - \phi\|_{L^2(\Omega)} + h\|\nabla(P_h\phi - \phi)\|_{L^2(\Omega)} \leq Ch^s \|\phi\|_{H^s(\Omega)}, \qquad s = 1, 2,$$

where the constant C is independent of the mesh parameter h. We also introduce the nodal interpolation operator

$$I_h : C(\overline{\Omega}) \to X_h,$$

which associates to each continuous function its piecewise linear interpolant. For every $v \in H^2(\Omega)$, the interpolation estimate

$$\|v - I_h v\|_{L^2(\Omega)} + h\|v - I_h v\|_{H^1(\Omega)} \leq Ch^2\|v\|_{H^2(\Omega)}$$

holds. These approximation properties will be essential in the derivation of the error estimates for the fully discrete scheme.

3.2.2 Temporal discretization

We now discretize the time interval $[0, T]$ uniformly by introducing the grid points

$$t_n = n\tau, \qquad n = 0, 1, \ldots, N, \qquad \tau = \frac{T}{N},$$

where τ denotes the time step size. Because the Caputo fractional derivative is nonlocal in time, classical time-stepping schemes are generally insufficient to capture the memory effects inherent in fractional diffusion equations. To overcome this difficulty, we employ convolution quadrature generated by the backward Euler method. The convolution quadrature method introduced by Lubich [25, 26] is employed for the temporal discretization of the fractional derivative. A modern presentation of convolution quadrature methods can be found in [2].

For a discrete sequence $\{\phi^n\}_{n=0}^N$, the discrete fractional derivative is defined by

$$\bar{\partial}_\tau^{\alpha(x)} \phi^n = \tau^{-\alpha(x)} \sum_{j=0}^{n} b_j^{(\alpha(x))} \phi^{n-j},$$

where the convolution weights $b_j^{(\alpha)}$ are determined through the generating relation

$$(1 - \xi)^\alpha = \sum_{j=0}^{\infty} b_j^{(\alpha)} \xi^j.$$

More precisely, the coefficients are given by $b_0^{(\alpha)} = 1$, and

$$b_j^{(\alpha)} = (-1)^j \frac{\alpha(\alpha - 1) \cdots (\alpha - j + 1)}{j!}, \qquad j \geq 1.$$

Remark 3.2.1 *This approximation replaces the history integral appearing in the Caputo derivative by a weighted discrete convolution sum while preserving the intrinsic memory structure of the fractional operator. Moreover, convolution quadrature methods are well known for their stability and consistency properties, making them particularly suitable for the numerical treatment of fractional evolution equations.*

3.2.3 Fully discrete forward scheme

We now combine the spatial finite element approximation with the temporal convolution quadrature discretization in order to derive a fully discrete formulation of the forward problem.

Recall that the weak formulation of the continuous problem is

$$(\partial_t^{\alpha(x)} u, v) + (\alpha \nabla u, \nabla v) = (f, v), \qquad \forall v \in H_0^1(\Omega).$$

Replacing the exact solution by its finite element approximation $U_h^n \in X_h$ and approximating the Caputo derivative by backward Euler convolution quadrature lead to the following fully discrete scheme. For each time level $n = 1, \ldots, N$, find $U_h^n \in X_h$ such that

$$(\bar{\partial}_\tau^{\alpha(x)}(U_h^n - U_h^0), \chi_h) + (\alpha \nabla U_h^n, \nabla \chi_h) = (f^n, \chi_h), \qquad \forall \chi_h \in X_h,$$

where $U_h^0 = P_h u_0$ is the projection of the initial condition onto the finite element space, and

$$f^n = \frac{1}{\tau} \int_{t_{n-1}}^{t_n} f(s)\, ds$$

denotes the averaged source term over the interval $[t_{n-1}, t_n]$. To simplify the notation, we introduce the discrete elliptic operator

$$A_h(\alpha) : X_h \to X_h$$

defined by

$$-(A_h(\alpha) v_h, \chi_h) = (\alpha \nabla v_h, \nabla \chi_h), \qquad \forall v_h, \chi_h \in X_h.$$

Using this operator, the fully discrete problem can be written compactly as

$$\bar{\partial}_\tau^{\alpha(x)}(U_h^n - U_h^0) - A_h(\alpha) U_h^n = P_h f^n, \qquad n = 1, \ldots, N.$$

The above formulation provides an efficient numerical procedure for approximating the solution of the forward problem at discrete time levels.

3.2.4 Discrete inverse problem

We next discretize the regularized inverse problem in order to obtain a finite-dimensional optimization problem suitable for numerical computation. Recall that the continuous Tikhonov functional is defined by

$$J_\gamma(\alpha) = \frac{1}{2}\|u(\alpha) - z^\delta\|^2_{L^2(0,T;L^2(\Omega))} + \frac{\gamma}{2}\|\nabla\alpha\|^2_{L^2(\Omega)}.$$

To derive a discrete counterpart, the time integral appearing in the data fidelity term is approximated by a quadrature formula. Using the rectangle rule, we replace $\int_0^T(\cdot)\,dt$ by $\tau\sum_{n=1}^N(\cdot)$. Consequently, the fully discrete Tikhonov functional is defined by

$$J_{\gamma,h,\tau}(\alpha_h) = \frac{\tau}{2}\sum_{n=1}^{N}\|U_h^n(\alpha_h) - z_n^\delta\|^2_{L^2(\Omega)} + \frac{\gamma}{2}\|\nabla\alpha_h\|^2_{L^2(\Omega)},$$

where $U_h^n(\alpha_h)$ denotes the fully discrete forward solution corresponding to the parameter α_h, and

$$z_n^\delta = \frac{1}{\tau}\int_{t_{n-1}}^{t_n} z^\delta(s)\,ds$$

represents the discrete observational data.

For improved temporal accuracy, one may alternatively employ the trapezoidal quadrature rule. In this case, the discrete functional becomes

$$J_{\gamma,h,\tau}(\alpha_h) = \frac{\tau}{2}\sum_{n=0}^{N} a_n\|U_h^n(\alpha_h) - z^\delta(t_n)\|^2_{L^2(\Omega)} + \frac{\gamma}{2}\|\nabla\alpha_h\|^2_{L^2(\Omega)},$$

where the quadrature weights are defined by

$$a_0 = a_N = \frac{1}{2}, \qquad a_n = 1, \quad 1 \le n \le N-1.$$

The discrete inverse problem therefore consists in solving

$$\min_{\alpha_h\in V_h} J_{\gamma,h,\tau}(\alpha_h).$$

Remark 3.2.2 *This formulation transforms the original infinite-dimensional inverse problem into a finite-dimensional optimization problem that can be efficiently solved using iterative numerical optimization algorithms.*

Lemma 3.2.3 (Stability of the discrete forward solver) *Let* $\{V_h^n\}_{n=0}^N \subset X_h$ *be the solution of the fully discrete problem*

$$(\bar{\partial}_\tau^{\alpha(x)} V_h^n, \chi_h) + (\alpha_h \nabla V_h^n, \nabla \chi_h) = (f_h^n, \chi_h), \qquad \forall \chi_h \in X_h,$$

with initial condition $V_h^0 = 0$. *Then the following stability estimate holds:*

$$\tau \sum_{n=1}^{N} \|\nabla V_h^n\|_{L^2(\Omega)}^2 \leq \frac{1}{\alpha_{\min}} \tau \sum_{n=1}^{N} (f_h^n, V_h^n).$$

Proof.

For each time level $n = 1, \ldots, N$, the discrete solution satisfies

$$(\bar{\partial}_\tau^{\alpha(x)} V_h^n, \chi_h) + (\alpha_h \nabla V_h^n, \nabla \chi_h) = (f_h^n, \chi_h), \qquad \forall \chi_h \in X_h.$$

To derive the stability estimate, we choose the test function $\chi_h = V_h^n$. Since $V_h^n \in X_h$, this choice is admissible and yields

$$(\bar{\partial}_\tau^{\alpha(x)} V_h^n, V_h^n) + (\alpha_h \nabla V_h^n, \nabla V_h^n) = (f_h^n, V_h^n).$$

Because $\alpha_h \in V_h \subset \mathcal{A}$, the admissibility condition implies $\alpha_h(x) \geq \alpha_{\min} > 0, \qquad$ a.e. in Ω. Therefore,

$$(\alpha_h \nabla V_h^n, \nabla V_h^n) = \int_\Omega \alpha_h(x) |\nabla V_h^n(x)|^2 \, dx \geq \alpha_{\min} \|\nabla V_h^n\|_{L^2(\Omega)}^2.$$

Next, we use the positivity property of the backward Euler convolution quadrature operator. Since the initial value satisfies $V_h^0 = 0$, we obtain

$$(\bar{\partial}_\tau^{\alpha(x)} V_h^n, V_h^n) \geq 0.$$

Combining the previous estimates gives

$$\alpha_{\min} \|\nabla V_h^n\|_{L^2(\Omega)}^2 \leq (f_h^n, V_h^n), \qquad n = 1, \ldots, N.$$

Multiplying both sides by the time step τ and summing over all time levels yields

$$\alpha_{\min}\tau\sum_{n=1}^{N}\|\nabla V_h^n\|^2_{L^2(\Omega)} \leq \tau\sum_{n=1}^{N}(f_h^n, V_h^n).$$

Finally, dividing by $\alpha_{\min}$ leads to

$$\tau\sum_{n=1}^{N}\|\nabla V_h^n\|^2_{L^2(\Omega)} \leq \frac{1}{\alpha_{\min}}\tau\sum_{n=1}^{N}(f_h^n, V_h^n),$$

which completes the proof.

■

Lemma 3.2.4 (Discrete Gronwall inequality for convolution quadrature) *Let $\{\phi^n\}_{n\geq 0}$ be a sequence in a Hilbert space, and let the backward Euler convolution quadrature operator be defined by*

$$\bar{\partial}_\tau^\alpha \psi^n = \tau^{-\alpha}\sum_{j=0}^{n} b_j^{(\alpha)}\psi^{n-j},$$

where the coefficients $b_j^{(\alpha)}$ are generated by

$$(1-\xi)^\alpha = \sum_{j=0}^{\infty} b_j^{(\alpha)}\xi^j.$$

Then the following inequality holds:

$$(\bar{\partial}_\tau^\alpha(\phi^n - \phi^0), \phi^n) \geq \frac{1}{2}\bar{\partial}_\tau^\alpha\left(\|\phi^n\|^2 - \|\phi^0\|^2\right).$$

Proof.

Starting from the definition of the convolution quadrature operator, we write

$$(\bar{\partial}_\tau^\alpha(\phi^n - \phi^0), \phi^n) = \tau^{-\alpha}\sum_{j=0}^{n} b_j^{(\alpha)}(\phi^{n-j} - \phi^0, \phi^n).$$

We now use the elementary identity valid in every Hilbert space:

$$2(a-b, a) = \|a\|^2 - \|b\|^2 + \|a-b\|^2.$$

Since the last term on the right-hand side is nonnegative, it follows that

$$(a-b, a) \geq \frac{1}{2}\big(\|a\|^2 - \|b\|^2\big).$$

Applying this relation with $a = \phi^n$ and $b = \phi^0$, yields

$$(\phi^n - \phi^0, \phi^n) \geq \frac{1}{2}\left(\|\phi^n\|^2 - \|\phi^0\|^2\right).$$

For the remaining terms corresponding to $j \geq 1$, we use the Cauchy-Schwarz inequality together with Young's inequality:

$$(\phi^{n-j}, \phi^n) \leq \frac{1}{2}\left(\|\phi^{n-j}\|^2 + \|\phi^n\|^2\right).$$

Consequently,

$$(\phi^{n-j} - \phi^0, \phi^n) \leq \frac{1}{2}\left(\|\phi^{n-j}\|^2 - \|\phi^0\|^2 + \|\phi^n\|^2\right).$$

Since the convolution quadrature coefficients satisfy

$$b_j^{(\alpha)} < 0, \qquad j \geq 1,$$

multiplication by $b_j^{(\alpha)}$ reverses the inequality and gives

$$b_j^{(\alpha)}(\phi^{n-j} - \phi^0, \phi^n) \geq \frac{1}{2} b_j^{(\alpha)}\left(\|\phi^{n-j}\|^2 - \|\phi^0\|^2 + \|\phi^n\|^2\right).$$

Summing over all indices $j = 0, \ldots, n$, we obtain

$$2(\bar{\partial}_\tau^\alpha(\phi^n - \phi^0), \phi^n) \geq \tau^{-\alpha} \sum_{j=0}^{n} b_j^{(\alpha)}\left(\|\phi^{n-j}\|^2 - \|\phi^0\|^2\right).$$

Observe that the right-hand side is precisely the discrete fractional derivative of the scalar sequence

$$g^n = \|\phi^n\|^2 - \|\phi^0\|^2.$$

Therefore,

$$2(\bar{\partial}_\tau^\alpha(\phi^n - \phi^0), \phi^n) \geq \bar{\partial}_\tau^\alpha\left(\|\phi^n\|^2 - \|\phi^0\|^2\right).$$

Finally, dividing by 2 yields

$$(\bar{\partial}_\tau^\alpha(\phi^n - \phi^0), \phi^n) \geq \frac{1}{2}\bar{\partial}_\tau^\alpha\left(\|\phi^n\|^2 - \|\phi^0\|^2\right),$$

which completes the proof.

■

Theorem 3.2.5 (Error estimate) *Let $\alpha \in \mathcal{A}$ be fixed, and let $u(\alpha)$ and $U_h^n(\alpha)$ denote respectively the exact solution of the forward problem and its fully discrete approximation. Assume that the exact solution possesses sufficient regularity. Then, for every $n = 1, \ldots, N$, the following estimate holds:*

$$\|u(\alpha)(t_n) - U_h^n(\alpha)\|_{L^2(\Omega)} \leq C\left(h^2 + \tau t_n^{\alpha_{\min}-1}\right),$$

where the constant C is independent of $h, \tau, n, \quad$ and $\quad \alpha \in \mathcal{A}$.

Proof.

Let $u(t) = u(\alpha)(t)$ denote the exact solution and let $U_h^n = U_h^n(\alpha)$ be the corresponding fully discrete approximation at time $t_n = n\tau$. We define the total error by

$$e^n = u(t_n) - U_h^n.$$

To estimate this quantity, we decompose the error into the form

$$e^n = \left(u(t_n) - P_h u(t_n)\right) + \left(P_h u(t_n) - U_h^n\right) = \rho^n + \theta^n,$$

where

$$\rho^n = u(t_n) - P_h u(t_n)$$

is the projection error and

$$\theta^n = P_h u(t_n) - U_h^n$$

is the discrete approximation error.

We first estimate the projection term. Since $u(t_n) \in H^2(\Omega)$, the approximation properties of the projection operator imply

$$\|\rho^n\|_{L^2(\Omega)} = \|u(t_n) - P_h u(t_n)\|_{L^2(\Omega)} \leq Ch^2 \|u(t_n)\|_{H^2(\Omega)} \leq Ch^2.$$

It therefore remains to estimate θ^n. The exact solution satisfies the variational identity

$$(\partial_t^{\alpha(x)} u(t_n), \chi_h) + (\alpha \nabla u(t_n), \nabla \chi_h) = (f(t_n), \chi_h), \qquad \forall \chi_h \in X_h.$$

On the other hand, the fully discrete solution satisfies

$$(\bar{\partial}_\tau^{\alpha(x)}(U_h^n - U_h^0), \chi_h) + (\alpha \nabla U_h^n, \nabla \chi_h) = (f^n, \chi_h), \qquad \forall \chi_h \in X_h.$$

Subtracting the two equations and using the fact that $P_h u(t_n) \in X_h$, we obtain the error equation

$$(\bar{\partial}_\tau^{\alpha(x)}\theta^n, \chi_h) + (\alpha\nabla\theta^n, \nabla\chi_h) = R^n(\chi_h),$$

where the residual term is given by

$$\begin{aligned} R^n(\chi_h) = &\left(\bar{\partial}_\tau^{\alpha(x)} P_h(u(t_n) - u_0) - \partial_t^{\alpha(x)} u(t_n), \chi_h\right) \\ &+ (f(t_n) - f^n, \chi_h) \\ &+ (\alpha\nabla(P_h u(t_n) - u(t_n)), \nabla\chi_h). \end{aligned}$$

Under the regularity assumptions imposed on the exact solution and the source term, standard estimates for backward Euler convolution quadrature yield

$$\left\| \bar{\partial}_\tau^{\alpha(x)}(u(t_n) - u_0) - \partial_t^{\alpha(x)} u(t_n) \right\|_{L^2(\Omega)} \leq C\tau t_n^{\alpha_{\min}-1}.$$

Since the projection operator P_h is bounded in $L^2(\Omega)$, the same estimate remains valid after projection. Moreover, the approximation properties of P_h imply

$$\|P_h \partial_t^{\alpha(x)} u(t_n) - \partial_t^{\alpha(x)} u(t_n)\|_{L^2(\Omega)} \leq Ch^2.$$

The quadrature approximation of the source term satisfies

$$\|f(t_n) - f^n\|_{L^2(\Omega)} \leq C\tau.$$

Finally, using the boundedness of α together with the approximation estimate for P_h, we obtain

$$|(\alpha\nabla(P_h u(t_n) - u(t_n)), \nabla\chi_h)| \leq Ch\|\nabla\chi_h\|_{L^2(\Omega)}.$$

Collecting the previous estimates yields

$$\|R^n\|_{L^2(\Omega)} \leq C\left(h^2 + \tau t_n^{\alpha_{\min}-1}\right).$$

We now choose $\chi_h = \theta^n$ in the error equation. This gives

$$(\bar{\partial}_\tau^{\alpha(x)}\theta^n, \theta^n) + (\alpha\nabla\theta^n, \nabla\theta^n) = R^n(\theta^n).$$

Using the positivity of the convolution quadrature operator together with the coercivity condition $\alpha(x) \geq \alpha_{\min} > 0$, we deduce

$$\alpha_{\min} \|\nabla \theta^n\|^2_{L^2(\Omega)} \leq \|R^n\|_{L^2(\Omega)} \|\theta^n\|_{L^2(\Omega)}.$$

Applying Poincaré's inequality yields

$$\|\theta^n\|_{L^2(\Omega)} \leq C \|\nabla \theta^n\|_{L^2(\Omega)}.$$

Consequently,

$$\|\theta^n\|_{L^2(\Omega)} \leq C \|R^n\|_{L^2(\Omega)}.$$

Using the estimate for the residual term, we conclude that

$$\|\theta^n\|_{L^2(\Omega)} \leq C \left(h^2 + \tau t_n^{\alpha_{\min}-1}\right).$$

Finally, combining the estimates for ρ^n and θ^n, we obtain

$$\begin{aligned} \|u(\alpha)(t_n) - U_h^n(\alpha)\|_{L^2(\Omega)} &\leq \|\rho^n\|_{L^2(\Omega)} + \|\theta^n\|_{L^2(\Omega)} \\ &\leq C \left(h^2 + \tau t_n^{\alpha_{\min}-1}\right). \end{aligned}$$

This completes the proof.

■

Theorem 3.2.6 (Convergence of discrete minimizers) *Let $\{\alpha_h^*\} \subset V_h$ be a sequence of minimizers of the discrete Tikhonov functional $J_{\gamma,h,\tau}$. Assume that the discrete forward solutions are consistent with the continuous forward problem and that the finite element spaces approximate the admissible set $\mathcal{A}$ in the sense that, for every $\alpha \in \mathcal{A}$, there exists a sequence $\alpha_h \in V_h$ such that*

$$\alpha_h \to \alpha \quad \textit{strongly in } H^1(\Omega).$$

Then there exist a subsequence, still denoted by $\{\alpha_h^*\}$, and a function $\bar{\alpha} \in \mathcal{A}$ such that

$$\alpha_h^* \rightharpoonup \bar{\alpha} \quad \textit{weakly in } H^1(\Omega),$$

and

$$\alpha_h^* \to \bar{\alpha} \quad \textit{strongly in } L^2(\Omega).$$

Moreover, $\bar{\alpha}$ is a minimizer of the continuous Tikhonov functional J_γ over $\mathcal{A}$.

Proof.

Let $\{\alpha_h^*\} \subset V_h$ be a sequence of discrete minimizers. Since $V_h \subset \mathcal{A}$, the box constraints imply

$$\alpha_{\min} \leq \alpha_h^*(x) \leq \alpha_{\max} \quad \text{a.e. in } \Omega.$$

Hence, $\{\alpha_h^*\}$ is uniformly bounded in $L^\infty(\Omega)$, and therefore also in $L^2(\Omega)$.

We next establish boundedness in $H^1(\Omega)$. Let $\alpha^\dagger \in \mathcal{A}$ be arbitrary. By the approximation property of the finite element spaces, there exists a sequence $\alpha_h^\dagger \in V_h$ such that

$$\alpha_h^\dagger \to \alpha^\dagger \quad \text{strongly in } H^1(\Omega).$$

By the minimality of α_h^*, we have

$$J_{\gamma,h,\tau}(\alpha_h^*) \leq J_{\gamma,h,\tau}(\alpha_h^\dagger).$$

The consistency of the discrete forward solver and the convergence of the quadrature approximation imply that the right-hand side is uniformly bounded with respect to h and τ. Thus, there exists a constant $C > 0$, independent of h and τ, such that

$$J_{\gamma,h,\tau}(\alpha_h^*) \leq C.$$

Since the data fidelity term is nonnegative, we obtain

$$\frac{\gamma}{2}\|\nabla \alpha_h^*\|_{L^2(\Omega)}^2 \leq J_{\gamma,h,\tau}(\alpha_h^*) \leq C.$$

Therefore,

$$\|\nabla \alpha_h^*\|_{L^2(\Omega)} \leq C.$$

Together with the L^2-boundedness, this proves that $\{\alpha_h^*\}$ is bounded in $H^1(\Omega)$.

Since $H^1(\Omega)$ is reflexive, there exist a subsequence, still denoted by $\{\alpha_h^*\}$, and a function $\bar{\alpha} \in H^1(\Omega)$ such that

$$\alpha_h^* \rightharpoonup \bar{\alpha} \quad \text{weakly in } H^1(\Omega).$$

Moreover, the compact embedding

$$H^1(\Omega) \hookrightarrow L^2(\Omega)$$

implies

$$\alpha_h^* \to \bar{\alpha} \quad \text{strongly in } L^2(\Omega).$$

Since $\mathcal{A}$ is weakly closed in $H^1(\Omega)$, we obtain $\bar{\alpha} \in \mathcal{A}$. It remains to prove that $\bar{\alpha}$ minimizes the continuous functional. Let $\alpha \in \mathcal{A}$ be arbitrary. By the approximation property, there exists a sequence $\alpha_h \in V_h$ such that

$$\alpha_h \to \alpha \quad \text{strongly in } H^1(\Omega).$$

Using again the minimality of α_h^*, we have

$$J_{\gamma,h,\tau}(\alpha_h^*) \leq J_{\gamma,h,\tau}(\alpha_h).$$

Passing to the upper limit as $h, \tau \to 0$, and using the consistency of the discrete functional, gives

$$\limsup_{h,\tau\to 0} J_{\gamma,h,\tau}(\alpha_h^*) \leq \limsup_{h,\tau\to 0} J_{\gamma,h,\tau}(\alpha_h) = J_\gamma(\alpha).$$

Since $\alpha \in \mathcal{A}$ was arbitrary, we obtain

$$\limsup_{h,\tau\to 0} J_{\gamma,h,\tau}(\alpha_h^*) \leq \inf_{\alpha\in\mathcal{A}} J_\gamma(\alpha).$$

On the other hand, by the weak lower semicontinuity of the H^1-seminorm, the continuity of the parameter-to-state map, and the convergence of the discrete forward solutions, we have

$$J_\gamma(\bar{\alpha}) \leq \liminf_{h,\tau\to 0} J_{\gamma,h,\tau}(\alpha_h^*).$$

Combining the last two inequalities yields

$$J_\gamma(\bar{\alpha}) \leq \inf_{\alpha\in\mathcal{A}} J_\gamma(\alpha).$$

Since $\bar{\alpha} \in \mathcal{A}$, the reverse inequality is immediate. Therefore,

$$J_\gamma(\bar{\alpha}) = \inf_{\alpha\in\mathcal{A}} J_\gamma(\alpha).$$

Thus, $\bar{\alpha}$ is a minimizer of the continuous Tikhonov functional over $\mathcal{A}$. Consequently, every sequence of discrete minimizers admits a subsequence converging weakly in $H^1(\Omega)$ and strongly in $L^2(\Omega)$ to a minimizer of the continuous regularized inverse problem.

This completes the proof.

■

3.3 Numerical reconstruction strategy

The numerical treatment of the inverse problem combines a finite element approximation of the forward model with a derivative-free optimization procedure. The spatial domain is discretized using continuous piecewise linear finite elements, while the variable-order fractional derivative is approximated by convolution quadrature. This yields a fully discrete model that provides the state solution corresponding to a given fractional-order distribution.

The reconstruction of the unknown parameter is formulated as the minimization of a discrete Tikhonov functional. Since the objective functional depends nonlinearly on the fractional order through the solution of the forward problem, an iterative optimization procedure is required.

In the present work, the minimization problem is solved using the Nelder–Mead simplex method [33], implemented in the `SciPy` optimization library [39]. This derivative-free optimization technique is particularly suitable for nonlinear inverse problems, as it does not require gradient information. At each iteration, the forward problem is solved, the objective functional is evaluated, and the parameter estimate is updated until convergence is achieved.

The resulting parameter is taken as the numerical approximation of the unknown space-dependent fractional order.

Algorithm 1: Finite element reconstruction of the fractional order

Input: Initial parameter estimate $\alpha^{(0)}$ and observation data Z_δ.
Output: Reconstructed fractional order α^*.
Construct the fully discrete finite element model.
Initialize the Nelder–Mead optimization algorithm.
while *the stopping criterion is not satisfied* **do**
    Solve the forward problem.
    Evaluate the Tikhonov functional.
    Update the parameter estimate using the Nelder–Mead method.
return α^*.

Chapter 4

Numerical Experiments

This chapter presents numerical experiments illustrating the reconstruction of the spatially varying fractional order in variable-order subdiffusion equations. The objective is to evaluate the effectiveness of the proposed numerical approaches for solving the inverse problem. Recent numerical reconstruction techniques for fractional-order inverse problems have been reported in [24].

First, the inverse problem is solved using the finite element optimization-based method developed in Chapter 3. Subsequently, a Physics-Informed Neural Network (PINN) framework is employed to reconstruct the unknown fractional order from observational data. Finally, the performance of the two approaches is compared in terms of reconstruction accuracy, convergence behavior, and computational efficiency.

4.1 Numerical reconstruction using the optimization-based method

4.1.1 Example 1:Reconstruction of a one-dimensional variable fractional order

In this first example, we investigate the reconstruction of a smooth spatially varying fractional order on the one-dimensional domain $\Omega = (0, 1)$. The exact coefficient is chosen as

$$\alpha^{\dagger}(x) = 0.3 + 0.4\sin(\pi x), \qquad x \in (0, 1),$$

while the initial condition is given by $u_0(x) = x(1 - x)$, and the source term is set to zero, $f(x, t) \equiv 0$. The final observation time is fixed to $T = 1$. Synthetic observations are generated by solving the forward problem using the exact fractional order and are subsequently employed as input data for the inverse problem.

The reconstruction starts from an initial constant approximation and is carried out using the optimization procedure described in Algorithm 1. At each iteration, the fully discrete forward problem is solved, the objective functional is evaluated, and the fractional order is updated until the prescribed stopping criterion is satisfied.

Figure 4.1 presents a comparison between the exact fractional order and the reconstructed solution obtained at convergence. The two curves are almost indistinguishable over most of the computational domain, demonstrating the ability of the proposed approach to recover the spatial variation of the unknown coefficient with high accuracy. In particular, the location of the maximum value and the overall sinusoidal profile are correctly identified.

To further assess the convergence of the optimization procedure, Figure 4.2 displays the evolution of the objective functional during the iterative process. A significant decrease is observed during the first iterations, followed by a slower reduction as the iterates approach the minimizer. This behavior is characteristic of gradient-based optimization methods and confirms the stability of the reconstruction procedure.

The evolution of the relative reconstruction error is shown in Figure 4.3. The error decreases rapidly during the initial iterations and eventually stabilizes at a very small

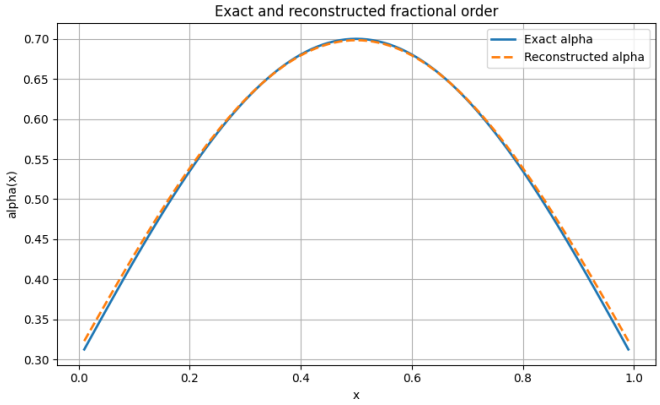

Figure 4.1: Exact and reconstructed fractional orders.

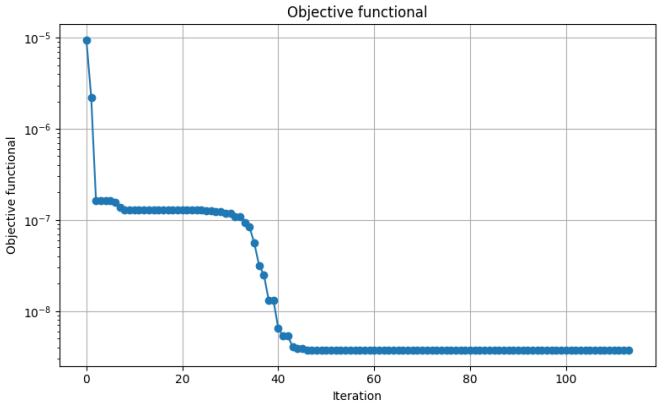

Figure 4.2: Evolution of the objective functional during the optimization process.

value. This confirms the convergence of the reconstructed coefficient toward the exact solution.

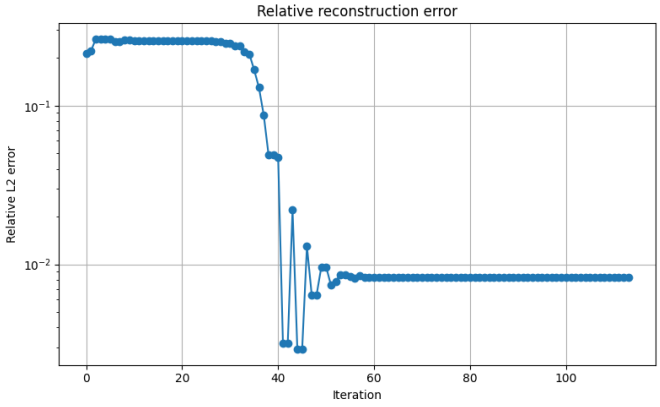

Figure 4.3: Evolution of the relative reconstruction error.

The optimization algorithm converged after 107 iterations. The final value of the objective functional was approximately

$$J^* = 3.6701 \times 10^{-9},$$

indicating an excellent agreement between the reconstructed state and the observed data. Moreover, the final relative reconstruction error was 8.3291×10^{-3}, while the corresponding absolute L^2 error was 4.7255×10^{-3}. These values demonstrate the high accuracy of the proposed inversion framework. The quantitative results are summarized in Table 4.1.

Quantity	Value
Number of iterations	107
Final objective functional	3.6701×10^{-9}
Relative L^2 error	8.3291×10^{-3}
Absolute L^2 error	4.7255×10^{-3}
Optimization status	Converged

Table 4.1: Numerical results.

Remark 4.1.1 *The results obtained in this first experiment demonstrate that the proposed finite element and convolution quadrature framework provides an accurate and stable reconstruction of smooth spatially dependent fractional orders. The excellent agreement between the exact and reconstructed coefficients, together with the small reconstruction error and the monotonic decrease of the objective functional, confirms the effectiveness of the proposed methodology.*

4.1.2 Example 2: Two-dimensional variable-order fractional diffusion problem

In this second example, we investigate the reconstruction of a spatially varying fractional order in the two-dimensional domain $\Omega = (0,1)^2$. The exact fractional order is chosen as

$$\alpha^\dagger(x,y) = 0.3 + 0.4\,\exp!\left(-10\big((x-0.5)^2 + (y-0.5)^2\big)\right), \qquad (x,y) \in \Omega,$$

which represents a smooth Gaussian bump centered at the middle of the domain. This configuration is particularly relevant because it allows us to evaluate the capability of the

reconstruction method to identify localized variations of the fractional order. The initial condition is prescribed by $u_0(x, y) = x(1 - x)\sin(\pi y)$, while the source term is taken to be $f(x, y, t) \equiv 0$. The final observation time is fixed to $T = 1$. The computational domain is discretized using a conforming triangular finite element mesh consisting of 625 nodes and 1152 triangular elements, resulting in 529 interior degrees of freedom. The temporal discretization is performed using the backward Euler convolution quadrature scheme described in the previous section. Synthetic observations are generated by solving the forward problem with the exact fractional order and are subsequently used as measurement data in the inverse problem.

Starting from an initial constant approximation, the optimization algorithm iteratively updates the fractional order until convergence is achieved. The evolution of the reconstruction process demonstrates a continuous reduction of both the objective functional and the reconstruction error. As the iterations progress, the reconstructed coefficient gradually approaches the exact Gaussian profile.

Figure 4.4 displays the exact fractional order distribution. The coefficient reaches its maximum value near the center of the domain and decreases smoothly toward the boundary. This smooth localized structure constitutes a challenging benchmark for the inverse problem because the reconstruction algorithm must simultaneously identify both the amplitude and the spatial location of the Gaussian peak.

Figure 4.5 presents the reconstructed fractional order obtained at convergence. A visual comparison with Figure 4.4 reveals an excellent agreement between the exact and reconstructed distributions. In particular, the reconstruction accurately captures the position, width, and magnitude of the Gaussian bump.

To further quantify the reconstruction quality, Figure 4.6 shows the pointwise absolute error distribution. The error remains very small throughout the computational domain and no significant localized artifacts are observed. This indicates that the proposed inversion framework provides a stable and accurate approximation of the unknown coefficient.

For a more detailed comparison, Figure 4.7 depicts the exact and reconstructed fractional orders along the horizontal centerline $y = 0.5$. The two curves are nearly indistin-

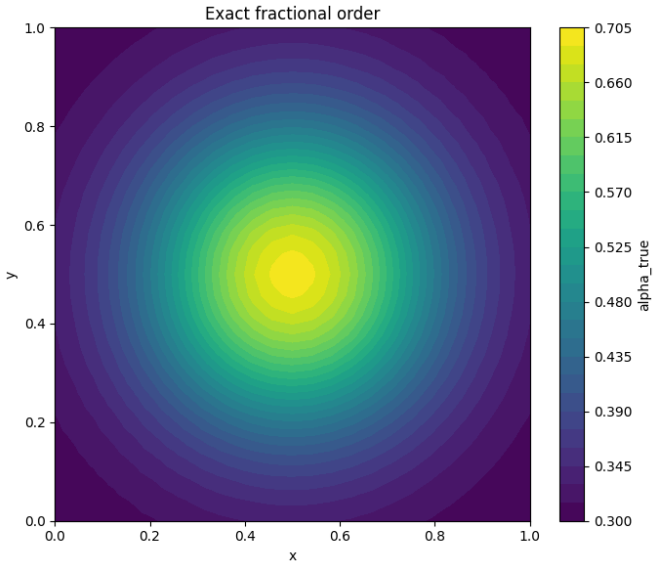

Figure 4.4: Exact fractional order $\alpha^{\dagger}(x, y)$.

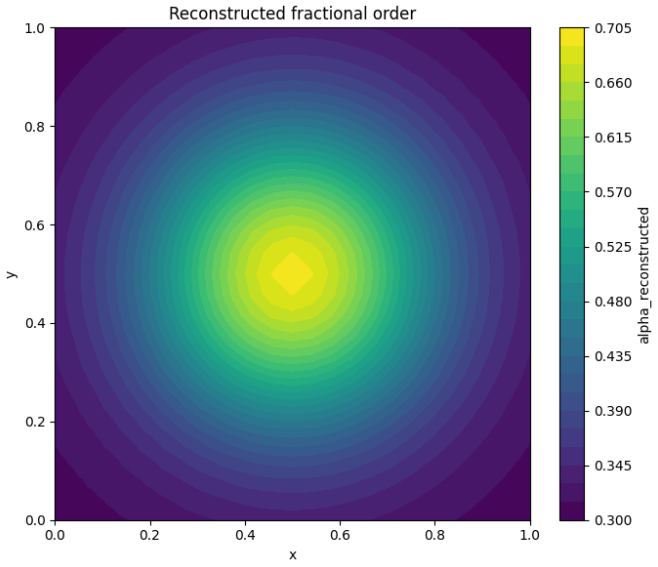

Figure 4.5: Reconstructed fractional order.

guishable, confirming the high accuracy of the reconstruction.

The convergence history of the objective functional is presented in Figure 4.8. A rapid decrease is observed during the first iterations, followed by a slower reduction as the iterates approach the minimizer. This behavior confirms the stability and efficiency of the optimization procedure.

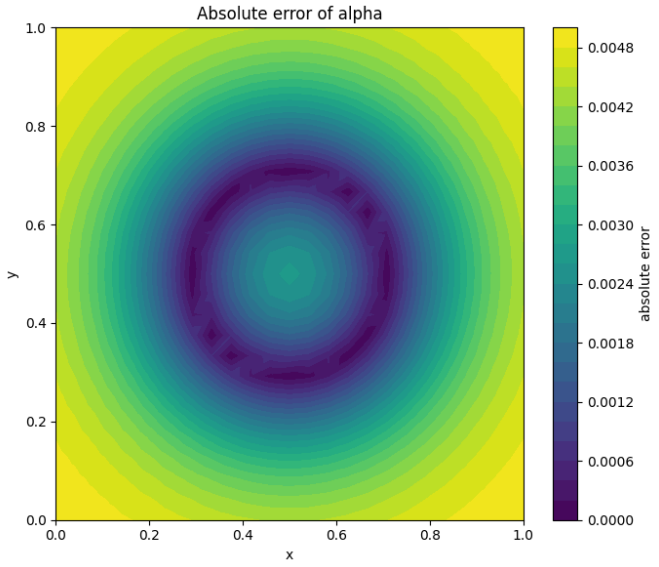

Figure 4.6: Pointwise absolute error of the reconstructed fractional order.

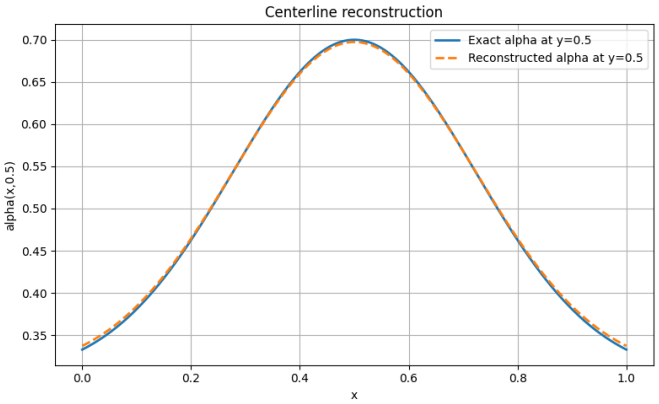

Figure 4.7: Comparison of the exact and reconstructed fractional orders along the centerline $y = 0.5$.

Similarly, Figure 4.9 illustrates the evolution of the relative reconstruction error. The error decreases steadily and eventually reaches a very small value, indicating convergence of the reconstructed parameter toward the exact solution.

The optimization algorithm converged successfully after 103 iterations. The final value of the objective functional was

$$J^* = 2.4052 \times 10^{-9},$$

while the relative and absolute reconstruction errors were 7.1650×10^{-3} and $3.0004 \times$

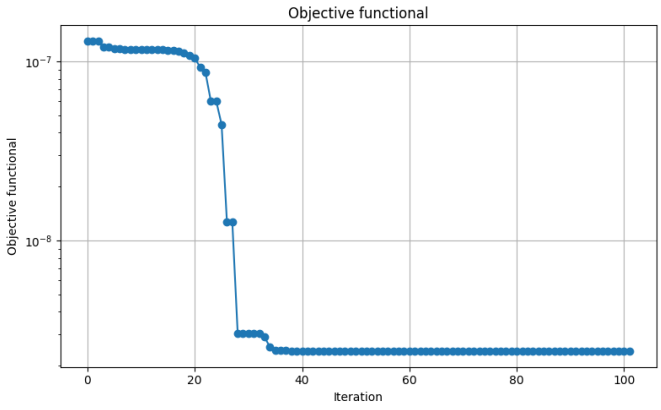

Figure 4.8: Evolution of the objective functional during the optimization process.

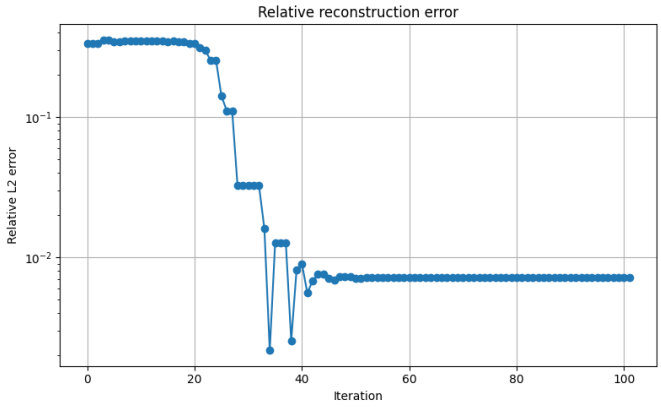

Figure 4.9: Evolution of the relative reconstruction error.

10^{-3}, respectively. These values demonstrate the excellent performance of the proposed reconstruction method. The main quantitative results are summarized in Table 4.2.

Quantity	Value
Number of nodes	625
Number of triangular elements	1152
Number of degrees of freedom	529
Number of optimization iterations	103
Final objective functional	2.4052×10^{-9}
Relative L^2 error	7.1650×10^{-3}
Absolute L^2 error	3.0004×10^{-3}
Optimization status	Converged

Table 4.2: Numerical results.

Remark 4.1.2 *The results obtained in this experiment confirm that the proposed finite*

element and convolution quadrature framework is capable of accurately reconstructing localized two-dimensional fractional orders. The excellent agreement between the exact and reconstructed Gaussian distributions, together with the small reconstruction errors and the monotonic decrease of the objective functional, demonstrate the robustness and effectiveness of the proposed inversion methodology.

4.2 Numerical examples via physics-informed neural networks

Physics-Informed Neural Networks (PINNs), introduced by Raissi, Perdikaris, and Karniadakis [36], constitute a powerful computational framework for solving partial differential equations (PDEs) through deep learning techniques. The fundamental idea behind PINNs is to incorporate the governing physical laws directly into the optimization process by penalizing the residual of the underlying differential equation through automatic differentiation. This approach provides mesh-free approximations for both forward and inverse problems, thereby avoiding the need for classical discretization methods.

Since their introduction, PINNs have been successfully applied to a wide variety of inverse problems involving parameter identification, source reconstruction, coefficient recovery, and fractional differential equations. In inverse settings, PINNs combine observational data with physics-based constraints in a unified optimization framework, offering an alternative to classical regularization techniques such as Tikhonov regularization [38]. Several recent works have demonstrated the efficiency of PINNs for recovering unknown coefficients and fractional parameters in anomalous diffusion and fractional dynamical systems [14, 35].

In recent years, considerable attention has been devoted to the application of PINNs to variable-order fractional differential equations, where the fractional order itself is unknown and must be identified from indirect observations. Such inverse problems are highly nonlinear and ill-posed, especially in multidimensional settings. Nevertheless, PINNs provide a flexible framework capable of simultaneously approximating both the solution and the unknown fractional order while maintaining consistency with the governing physical

model.

4.2.1 General PINN framework for inverse fractional-order problems

Before presenting the numerical results for the one-dimensional and two-dimensional examples, we briefly describe the general PINN framework used for the recovery of the unknown fractional order.

The main objective is to simultaneously approximate the state variable and the unknown variable fractional order appearing in the governing fractional diffusion equation. In both examples, this is achieved by combining neural network approximation with a physics-informed learning strategy in which the differential equation, initial conditions, boundary conditions, and observational data are incorporated into a unified loss functional.

4.2.2 Neural network structure and layer representation

We consider a feedforward neural network $\mathcal{N}_\theta$ that maps the space–time variables to the unknown quantities of interest. In the general setting, this mapping is written as

$$\mathcal{N}_\theta : (\mathbf{x}, t) \mapsto \big(u_\theta(\mathbf{x}, t), \alpha_\theta(\mathbf{x})\big),$$

where θ denotes the collection of trainable parameters.

Layer-wise construction. The neural network consists of:

- an input layer representing the variables $(\mathbf{x}, t)$,
- several hidden layers equipped with nonlinear activation functions,
- an output layer approximating the state solution u and the fractional order α.

More precisely, the network is recursively defined by

$$z^{(0)} = (\mathbf{x}, t),$$

$$z^{(\ell)} = \rho\left(W^{(\ell)} z^{(\ell-1)} + b^{(\ell)}\right), \qquad \ell = 1, \ldots, L-1,$$
$$\mathcal{N}_\theta(\mathbf{x}, t) = W^{(L)} z^{(L-1)} + b^{(L)},$$

where $W^{(\ell)}$ and $b^{(\ell)}$ denote the weights and biases of the network, ρ is a nonlinear activation function (chosen here as `tanh`), and L represents the total number of layers.

This architecture allows the neural network to act as a universal approximator for both the solution and the unknown fractional order. The approximation properties of deep neural networks in Sobolev spaces and related function classes have been extensively studied in the literature; see, for example, [44].

Interpretation of the layers.

- Input layer: encodes the space–time coordinates $(\mathbf{x}, t)$.
- Hidden layers: extract nonlinear features associated with diffusion behavior and fractional dynamics.
- Output layer: provides approximations of the state solution u and the fractional order α.

The hidden layers therefore provide a shared latent representation that enables the simultaneous reconstruction of all unknown quantities.

4.2.3 Diagram of the PINN architecture

The general architecture of the PINN employed for the inverse fractional-order problem is illustrated in Figure 4.10.

4.2.4 Physics-informed formulation

The neural network is trained by minimizing a composite loss functional:

$$\mathcal{L}(\theta) = \mathcal{L}_{\text{PDE}} + \mathcal{L}_{\text{data}} + \mathcal{L}_{\text{IC}} + \mathcal{L}_{\text{BC}} + \lambda \mathcal{L}_\alpha.$$

Here:

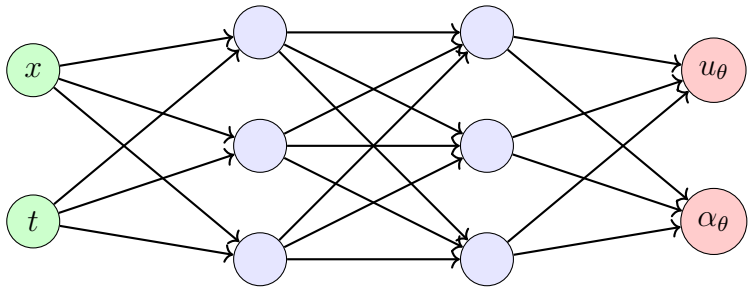

Figure 4.10: General architecture of the PINN for inverse fractional-order problems. The network maps space–time inputs to the state solution and the unknown fractional order.

- $\mathcal{L}_{\text{PDE}}$ penalizes the residual of the governing fractional differential equation,
- $\mathcal{L}_{\text{data}}$ enforces agreement with observational data,
- $\mathcal{L}_{\text{IC}}$ and $\mathcal{L}_{\text{BC}}$ impose the initial and boundary conditions,
- $\mathcal{L}_{\alpha}$ represents a regularization term associated with the unknown fractional order.

The PDE residual is computed using automatic differentiation:

$$\mathcal{R}_\theta = \mathcal{F}\big(u_\theta, \alpha_\theta\big),$$

where $\mathcal{F}$ denotes the governing variable-order fractional diffusion operator. This formulation may be viewed as a neural counterpart of a Tikhonov-type regularization framework, where the regularization term contributes to the stability of the inverse problem. The physics-informed structure of the loss functional plays a crucial role in stabilizing the inverse reconstruction process, particularly in the presence of limited observational data. By enforcing consistency with the governing fractional PDE, the PINN acts as an implicit regularization mechanism.

4.2.5 Training strategy

The training procedure employed in both numerical examples relies on three sets of sampling points:

- collocation points distributed inside the space–time domain,

- points enforcing the initial and boundary conditions,
- observational points corresponding to available measurement data.

The optimization process is performed in two stages:

- an initial stochastic optimization stage using the Adam optimizer,
- a deterministic refinement stage using the L-BFGS algorithm.

This hybrid optimization strategy improves both convergence and reconstruction accuracy.

4.2.6 General remarks

The same PINN framework is used for both the one-dimensional and two-dimensional inverse fractional-order problems. The differences arise only from:

- the spatial dimensionality,
- the structure of the governing fractional PDE,
- the parametrization of the unknown fractional order.

Consequently, PINNs provide a unified and mesh-free framework for solving inverse problems involving variable-order fractional differential equations while preserving consistency with the underlying physical laws through the explicit incorporation of the governing equations into the loss functional.

4.2.7 Example 1: Reconstruction of a one-dimensional variable fractional order

In this example, we investigate the inverse recovery of a spatially varying fractional order in a one-dimensional subdiffusion equation using a Physics-Informed Neural Network (PINN). The objective is to simultaneously reconstruct the unknown fractional order $\alpha(x)$ and the corresponding state solution $u(x,t)$ from synthetic observational data.

We consider the following variable-order fractional diffusion problem:

$$\partial_t^{\alpha(x)} u(x,t) - u_{xx}(x,t) = 0, \qquad (x,t) \in (0,1) \times (0,1],$$

subject to the homogeneous Dirichlet boundary conditions

$$u(0,t) = u(1,t) = 0, \qquad t \in (0,1],$$

and the initial condition

$$u(x,0) = x(1-x), \qquad x \in (0,1).$$

The exact fractional order is prescribed by

$$\alpha_{\text{true}}(x) = 0.3 + 0.4\sin(\pi x),$$

which varies smoothly over the spatial domain and attains its maximum value near the center of the interval.

The synthetic observations are generated numerically using a finite difference discretization combined with the L1 approximation of the Caputo fractional derivative. These observations are then used to train the PINN model.

Reconstruction accuracy

The reconstruction errors are measured using the relative L^2 norm:

$$\text{Error}(\alpha) = \frac{\|\alpha_{\text{pred}} - \alpha_{\text{true}}\|}{\|\alpha_{\text{true}}\|},$$

and

$$\text{Error}(u) = \frac{\|u_{\text{pred}} - u_{\text{true}}\|}{\|u_{\text{true}}\|}.$$

The obtained numerical errors are:

$$\frac{\|\alpha - \alpha_{\text{true}}\|_{L^2}}{\|\alpha_{\text{true}}\|_{L^2}} = 5.4251 \times 10^{-3},$$

and

$$\frac{\|u - u_{\text{true}}\|_{L^2}}{\|u_{\text{true}}\|_{L^2}} = 5.8749 \times 10^{-2}.$$

These results indicate that the proposed PINN framework successfully reconstructs both the unknown fractional order and the corresponding state solution with high accuracy.

Recovery of the fractional order

Figure 4.11 illustrates the exact and reconstructed fractional orders.

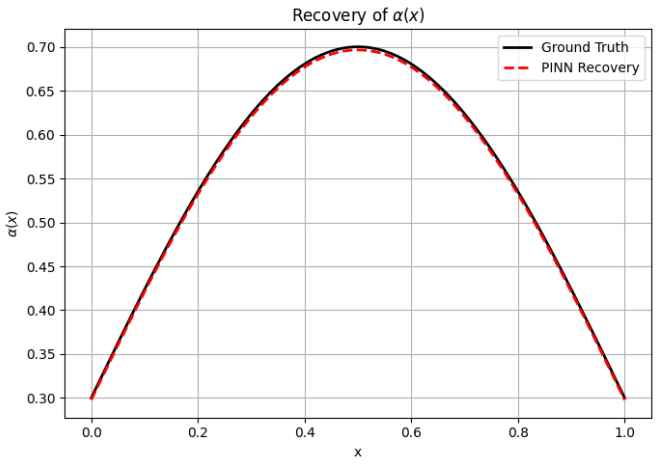

Figure 4.11: Exact and reconstructed fractional orders $\alpha(x)$.

The comparison between the exact and reconstructed fractional orders shown in Figure 4.11 demonstrates an excellent agreement over the entire spatial domain. The PINN accurately captures both the amplitude and the shape of the exact profile. No significant oscillations or local distortions are observed, indicating that the network successfully identifies the underlying spatial variation of the fractional order.

The relative reconstruction error remains very small, confirming the effectiveness of the proposed PINN framework for inverse identification of variable-order fractional parameters.

Figure 4.12 presents the absolute reconstruction error of the fractional order. The error remains uniformly small throughout the domain and does not exceed 3.6×10^{-3}. The error distribution is nearly symmetric with respect to the midpoint of the interval, reflecting the symmetry of the exact fractional-order function.

These results indicate that the PINN not only reproduces the global behavior of the coefficient but also achieves a highly accurate pointwise reconstruction.

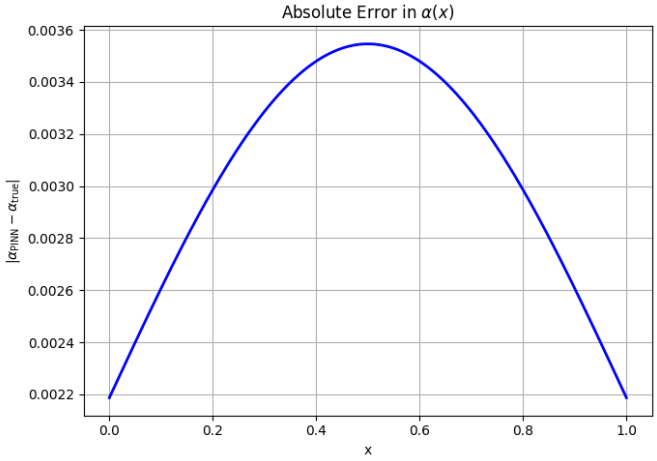

Figure 4.12: Absolute reconstruction error of $\alpha(x)$.

x	$\lvert\alpha_{\text{pred}} - \alpha_{\text{true}}\rvert$
0.0000	2.186626×10^{-3}
0.1106	2.649277×10^{-3}
0.2211	3.056705×10^{-3}
0.3317	3.360271×10^{-3}
0.4422	3.523588×10^{-3}
0.5578	3.523588×10^{-3}
0.6683	3.360212×10^{-3}
0.7789	3.056765×10^{-3}
0.8894	2.649307×10^{-3}
1.0000	2.186626×10^{-3}

Table 4.3: Absolute error in the recovered fractional order $\alpha(x)$ at selected spatial points.

Table 4.3 reports the absolute error between the recovered fractional order and the exact fractional order at selected spatial locations. The error remains uniformly small over the entire spatial domain, with a maximum value of approximately 3.52×10^{-3}. The symmetric distribution of the error reflects the symmetric structure of the exact fractional-order function. These results demonstrate that the proposed PINN-based inverse reconstruction accurately identifies the space-dependent fractional order and provides an excellent approximation of the exact parameter throughout the domain.

Reconstruction of the state variable

The exact and reconstructed solutions over the space-time domain are displayed in Figure 4.13.

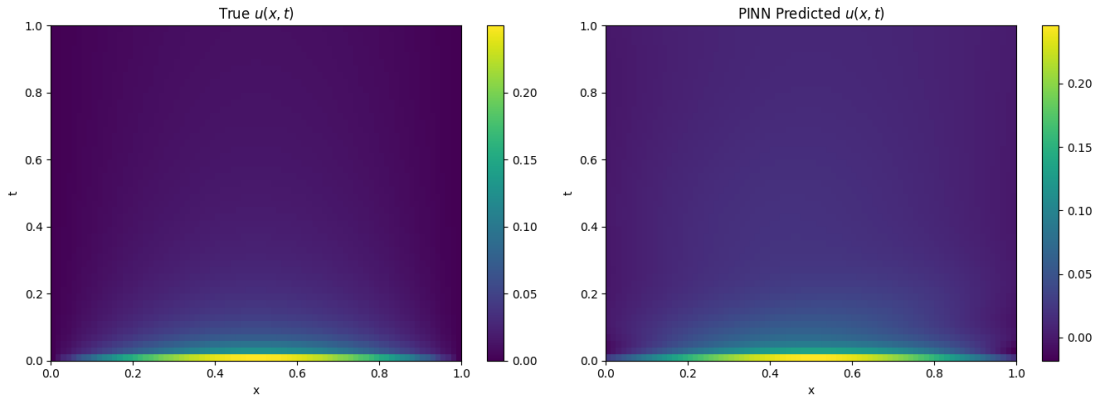

Figure 4.13: Exact solution $u(x,t)$ (left) and reconstructed solution (right).

The reconstructed solution remains in close agreement with the reference solution throughout the entire space–time domain, indicating that the PINN successfully captures the temporal evolution of the subdiffusion process.

The absolute reconstruction error over the space-time domain is presented in Figure 4.14.

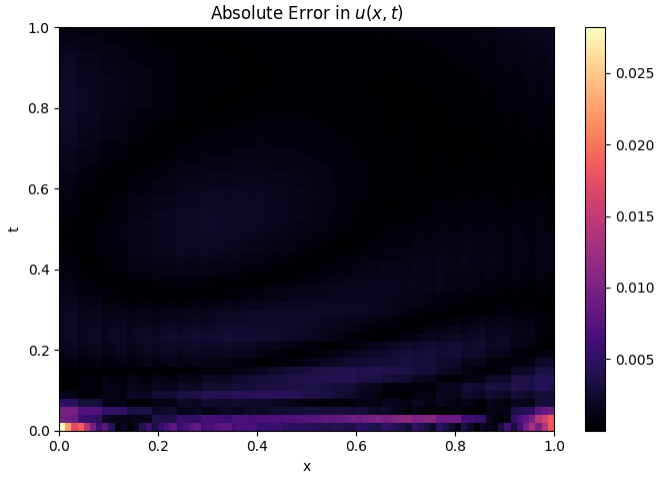

Figure 4.14: Absolute error $|u_{\text{true}} - u_{\text{pred}}|$ over the space–time domain.

The largest error occurs near the initial time layer, while the error decreases significantly as time evolves.

Temporal solution snapshots

To further evaluate the reconstruction accuracy, several temporal snapshots are considered.

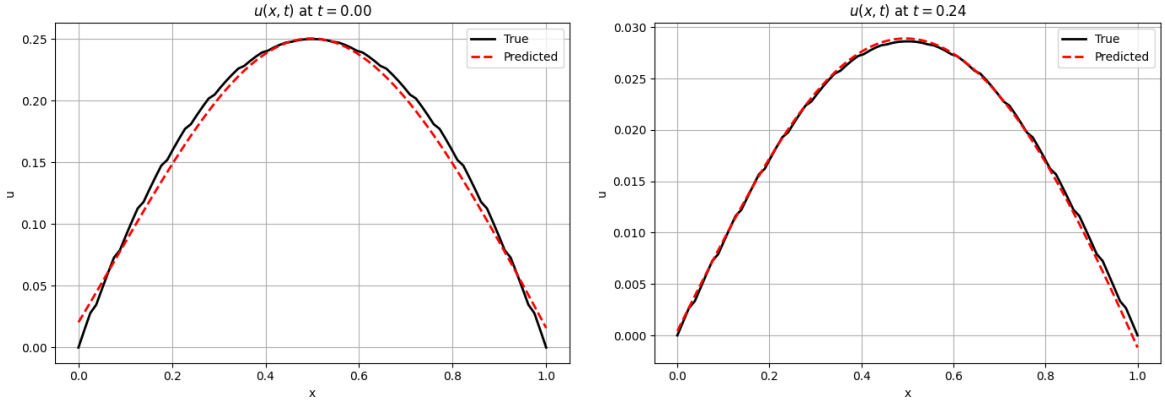

Figure 4.15: Comparison between exact and reconstructed solutions at $t = 0$ (left) and $t \approx 0.24$ (right).

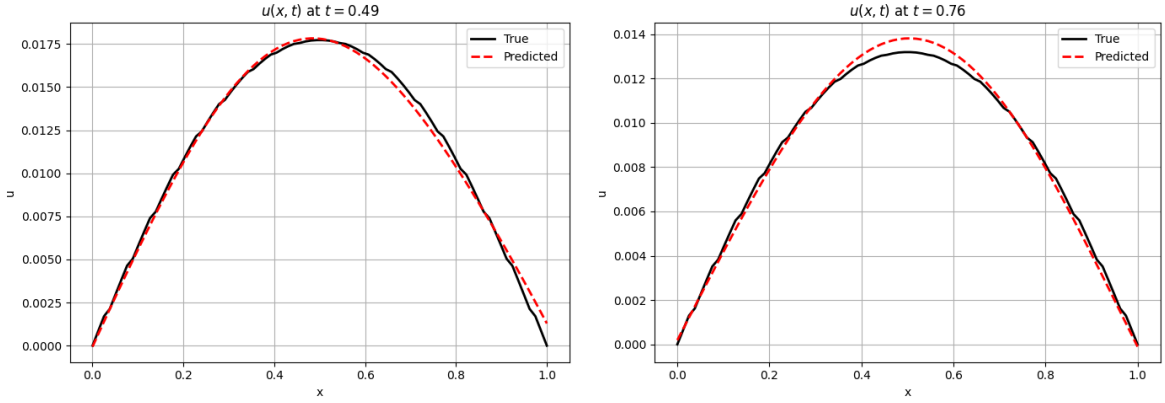

Figure 4.16: Comparison between exact and reconstructed solutions at $t \approx 0.49$ (left) and $t \approx 0.76$ (right).

The numerical results demonstrate excellent agreement between the exact and reconstructed solutions at all considered time levels.

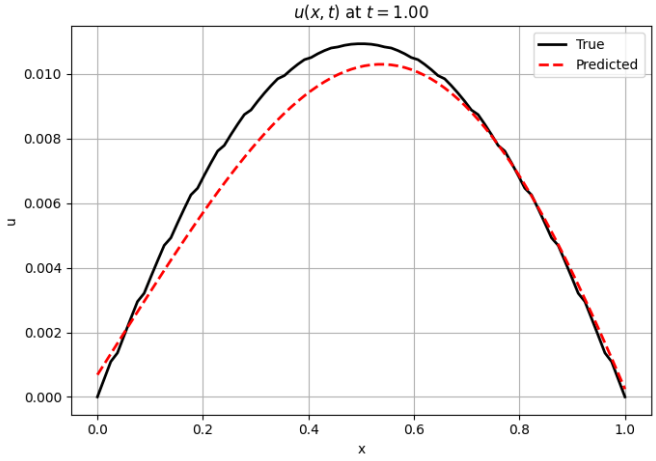

Figure 4.17: Comparison between exact and reconstructed solutions at final time $t = 1$.

Final-time error analysis

The absolute reconstruction error at the final time is illustrated in Figure 4.18.

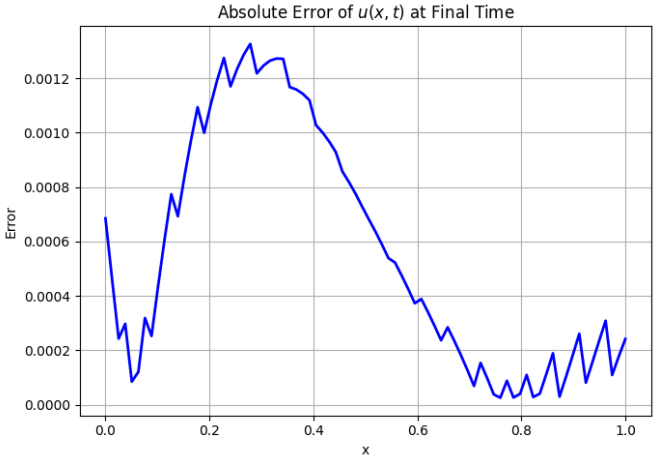

Figure 4.18: Absolute error of $u(x,t)$ at the final time.

The error remains very small over the entire spatial interval, which further confirms the accuracy of the proposed PINN reconstruction.

The mean absolute error at selected time levels is reported in Table **??**.

t	Mean Absolute Error in u
0.0000	6.131117×10^{-3}
0.1020	2.170453×10^{-3}
0.2245	1.694015×10^{-3}
0.3265	8.441253×10^{-4}
0.4490	9.929960×10^{-4}
0.5510	9.130247×10^{-4}
0.6735	5.524916×10^{-4}
0.7755	4.851391×10^{-4}
0.8980	5.352447×10^{-4}
1.0000	5.773152×10^{-4}

Table 4.4: Mean absolute error of the recovered state variable $u(x,t)$ at selected time values.

Table 4.4 presents the mean absolute error of the reconstructed state variable $u(x,t)$ at selected time levels. The results indicate that the reconstruction error decreases rapidly after the initial time and remains below 2.2×10^{-3} throughout the simulation. For most time instances, the error is of the order of 10^{-4} to 10^{-3}, demonstrating the high accuracy of the proposed PINN-based reconstruction method. The small magnitude of the error confirms that the recovered solution closely matches the reference solution over the entire time interval.

Discussion. The numerical results demonstrate the ability of the proposed PINN methodology to accurately recover both the unknown fractional order and the associated state solution from observation data. The reconstructed coefficient closely matches the exact fractional-order distribution, with a relative error of order 10^{-3}.

The absolute error remains uniformly small across the computational domain, showing that the network successfully captures both the global and local characteristics of the coefficient. Moreover, the reconstructed state solution exhibits excellent agreement with the reference solution, indicating that the physical constraints incorporated into the loss function effectively guide the training process.

Overall, the results confirm that PINNs provide a reliable and accurate framework for solving inverse variable-order fractional diffusion problems in one spatial dimension.

4.2.8 Example 2: Two-dimensional variable-order fractional diffusion problem

In this example, we investigate the inverse recovery of a spatially varying fractional order in a two-dimensional variable-order time-fractional diffusion equation. The reconstruction is carried out using a Physics-Informed Neural Network (PINN), where both the state solution $u(x, y, t)$ and the unknown fractional order $\alpha(x, y)$ are simultaneously approximated from synthetic observation data.

We consider the problem

$$\partial_t^{\alpha(x,y)} u(x, y, t) - \Delta u(x, y, t) = 0, \qquad (x, y, t) \in (0, 1)^2 \times (0, 1],$$

subject to homogeneous Dirichlet boundary conditions

$$u(x, y, t) = 0, \qquad (x, y) \in \partial\Omega,$$

and the initial condition

$$u(x, y, 0) = x(1 - x) \sin(\pi y).$$

The exact variable fractional order is chosen as

$$\alpha_{\text{true}}(x, y) = 0.3 + 0.4 \exp\left(-10\left[(x - 0.5)^2 + (y - 0.5)^2\right]\right).$$

This coefficient has a Gaussian-type profile centered at $(0.5, 0.5)$, where the largest fractional order values occur near the center of the spatial domain.

Reconstruction errors

The reconstruction quality is evaluated using the relative L^2 error:

$$\text{Error}(\alpha) = \frac{\|\alpha_{\text{pred}} - \alpha_{\text{true}}\|}{\|\alpha_{\text{true}}\|},$$

and

$$\text{Error}(u) = \frac{\|u_{\text{pred}} - u_{\text{true}}\|}{\|u_{\text{true}}\|}.$$

The obtained numerical errors are

$$\frac{\|\alpha - \alpha_{\text{true}}\|_{L^2}}{\|\alpha_{\text{true}}\|_{L^2}} = 6.7795 \times 10^{-3},$$

and

$$\frac{\|u - u_{\text{true}}\|_{L^2}}{\|u_{\text{true}}\|_{L^2}} = 2.4616 \times 10^{-1}.$$

Although the problem is considerably more challenging than the one-dimensional case, the PINN still captures the principal spatial structure of both the unknown coefficient and the state solution.

Recovery of the fractional order

Figure 4.19 display the exact and reconstructed fractional orders.

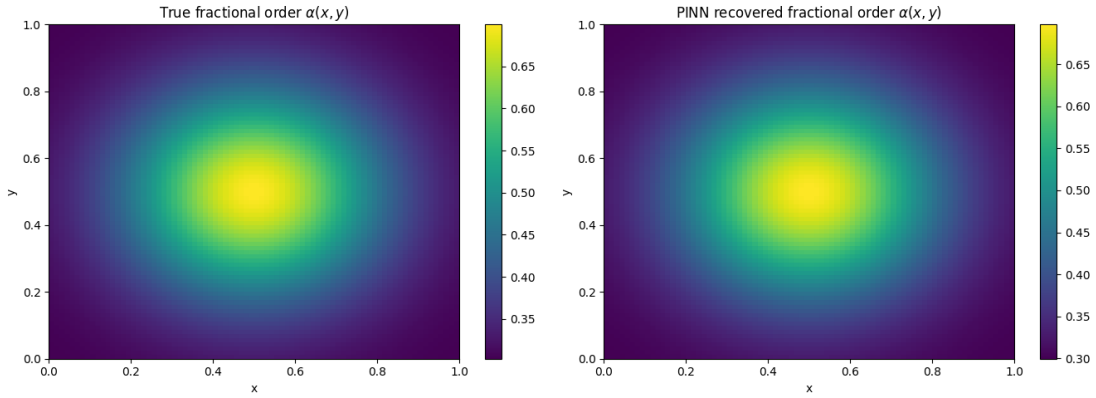

Figure 4.19: Exact fractional order $\alpha(x, y)$ (left) and reconstructed fractional order (right).

The reconstructed coefficient reproduces the global Gaussian profile and correctly identifies the region where the fractional order reaches its maximum.

The absolute reconstruction error of $\alpha(x, y)$ is shown in Figure 4.20.

The largest reconstruction error occurs near the central region where the coefficient changes more rapidly.

Centerline analysis of the fractional order

To further analyze the reconstruction quality, we consider the centerline $y = 0.5$. Figure 4.21 compares the exact and reconstructed fractional orders along this line.

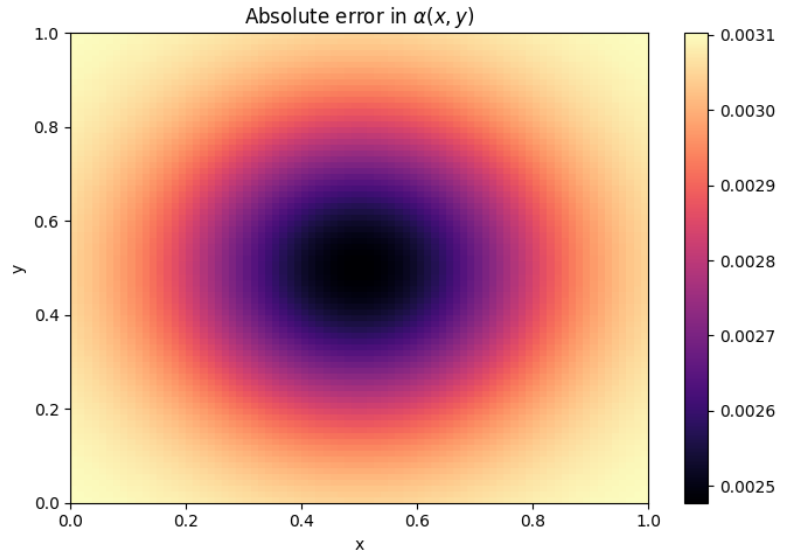

Figure 4.20: Absolute reconstruction error of $\alpha(x, y)$.

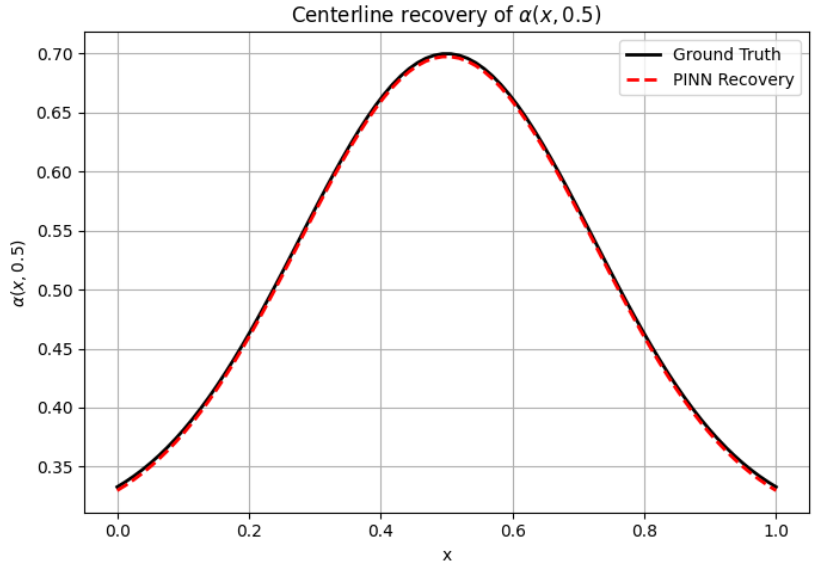

Figure 4.21: Comparison between the exact and reconstructed fractional orders along the centerline $y = 0.5$.

The corresponding absolute error along the centerline is shown in Figure 4.22.

Table 4.5 presents the absolute reconstruction error at selected spatial points.

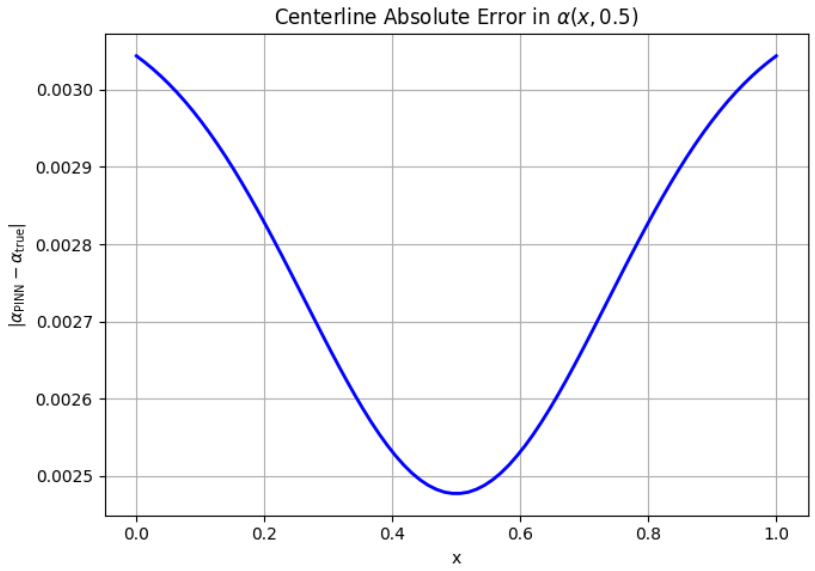

Figure 4.22: Absolute reconstruction error of $\alpha(x, 0.5)$.

x	$\lvert\alpha_{\text{pred}} - \alpha_{\text{true}}\rvert$
0.0000	3.043503×10^{-3}
0.1139	2.944380×10^{-3}
0.2278	2.784342×10^{-3}
0.3291	2.622724×10^{-3}
0.4430	2.495289×10^{-3}
0.5570	2.495289×10^{-3}
0.6709	2.622724×10^{-3}
0.7722	2.784342×10^{-3}
0.8861	2.944380×10^{-3}
1.0000	3.043503×10^{-3}

Table 4.5: Absolute error in the recovered fractional order along the centerline $y = 0.5$.

Temporal error statistics

Table 4.6 reports the mean absolute reconstruction error of the state solution at selected time levels.

Discussion. The numerical results demonstrate that the proposed PINN framework successfully reconstructs both the spatially varying fractional order and the corresponding state solution in two dimensions.

t	Mean Absolute Error in u
0.0000	2.075290×10^{-2}
0.1333	4.019800×10^{-3}
0.2000	3.749143×10^{-3}
0.3333	3.525963×10^{-3}
0.4667	2.996947×10^{-3}
0.5333	2.389690×10^{-3}
0.6667	1.779767×10^{-3}
0.8000	1.419145×10^{-3}
0.8667	1.290720×10^{-3}
1.0000	3.082582×10^{-3}

Table 4.6: Mean absolute error of the recovered state variable $u(x, y, t)$ at selected time values.

The reconstructed coefficient accurately reproduces the Gaussian profile of the exact fractional order and correctly identifies the location and magnitude of the maximum value. Although the inverse problem becomes more challenging in two dimensions, the reconstruction error remains below one percent, indicating a high level of accuracy.

The centerline analysis and the error distributions further confirm that the recovered parameter preserves the main spatial features of the exact coefficient. These results illustrate the robustness and effectiveness of the PINN methodology for multidimensional inverse variable-order fractional diffusion problems.

4.3 Comparison between the optimization-based method and physics-informed neural networks

In this section, we compare the optimization-based reconstruction method presented in Section 4.1 with the physics-informed neural network (PINN) approach introduced in Section 4.2. Both methods were applied to the inverse problem of recovering a spatially varying fractional order from observation data.

The numerical experiments demonstrate that both approaches are capable of accurately reconstructing the unknown fractional-order distribution and the corresponding state solution. In the examples considered in this work, the optimization-based method

and the PINN approach both achieved highly accurate reconstructions, with relative errors remaining small in both one-dimensional and two-dimensional settings.

From a computational perspective, the optimization-based approach requires the repeated solution of the forward problem throughout the iterative minimization process. Consequently, the computational cost generally increases with mesh refinement and the number of optimization iterations. In contrast, PINNs avoid repeated mesh-based PDE solves by embedding the governing equation directly into the training process. Although neural-network training may require a large number of epochs, the computations can be efficiently parallelized on modern GPU architectures.

Regarding flexibility, the optimization-based method relies on a complete numerical discretization of the governing equation and often requires the derivation of sensitivity or adjoint information. This provides a rigorous mathematical framework and allows for a precise treatment of the inverse problem. On the other hand, PINNs integrate the differential equation, boundary conditions, initial conditions, and observation data into a unified loss functional, making them particularly attractive for complex geometries, irregular data distributions, and high-dimensional problems.

An additional advantage of PINNs is their mesh-free nature, which simplifies the treatment of multidimensional inverse problems. However, the performance of PINNs may depend on the network architecture, the choice of hyperparameters, and the balance between the different components of the loss function. In contrast, optimization-based approaches benefit from a more mature theoretical foundation and well-established convergence analyses.

Overall, both methodologies provide effective tools for the identification of variable fractional orders. The optimization-based method offers a rigorous mathematical framework and reliable reconstruction performance, while PINNs provide remarkable flexibility and scalability. The numerical results obtained in this work indicate that PINNs constitute a competitive alternative for solving inverse variable-order fractional diffusion problems, particularly when dealing with complex or high-dimensional settings.

Remark 4.3.1 *The reconstruction quality obtained with PINNs may be further enhanced*

by incorporating additional prior information on the unknown fractional order. For example, smoothness constraints, monotonicity conditions, bounded variation assumptions, or other physically motivated regularization strategies can be included in the loss function to improve both reconstruction accuracy and training stability.

Aspect	**Optimization-based method**	**PINN method**
Accuracy	Very high reconstruction accuracy	Very high reconstruction accuracy in the considered examples
Computational effort	Repeated forward solves during optimization	Neural-network training
Flexibility	Requires numerical discretization	Mesh-free and easily adaptable
High-dimensional problems	Can become computationally demanding	Naturally suited for high-dimensional settings
Theoretical foundation	Well established	Rapidly developing
Implementation	Requires PDE solver and optimization framework	Requires network design and training strategy

Table 4.7: Comparison between the optimization-based method and PINNs.

Conclusion and some perspectives

In this work, we have investigated an inverse problem associated with a variable-order time-fractional diffusion equation. The main objective was to reconstruct an unknown spatially varying fractional order from observational data.

First, the mathematical framework of the forward problem was established, and the existence, uniqueness, regularity, and continuity properties of the corresponding weak solution were investigated. The inverse problem of identifying the space-dependent fractional order was then formulated as a Tikhonov-regularized optimization problem to overcome its ill-posedness. For the numerical solution, a finite element method combined with convolution quadrature was developed for the discretization of the forward model, and the resulting minimization problem was solved using the Nelder–Mead optimization algorithm. Numerical experiments performed in one- and two-dimensional settings demonstrated the effectiveness of the proposed approach and its ability to accurately reconstruct the unknown fractional order from observational data.

In addition, Physics-Informed Neural Networks (PINNs) were applied to the same inverse problem. Numerical experiments showed that PINNs provide an effective mesh-free alternative for parameter identification. The numerical results obtained in this thesis confirm the feasibility of reconstructing variable fractional orders from measurement data. Both the optimization-based method and the Physics-Informed Neural Network (PINN)

approach successfully recover the unknown coefficient and provide accurate approximations of the exact solution. These results demonstrate the effectiveness of the proposed methodologies for inverse fractional diffusion problems and highlight the potential of combining mathematical modeling, numerical analysis, and machine-learning techniques in the study of fractional-order systems.

Some perspectives

Several directions may be considered for future research:

- Simultaneous reconstruction of multiple unknown parameters.
- Extension to nonlinear and three-dimensional fractional diffusion models.
- Development of adaptive and more efficient numerical algorithms.
- Construction of hybrid methods combining optimization techniques and PINNs.
- Exploration of advanced neural-network architectures for inverse fractional problems.

The present work provides a solid basis for further developments in the analysis and numerical solution of inverse problems governed by variable-order fractional differential equations.

Bibliography

[1] K. S. Agbodjan, O. S. Ahmed, D. Messaoudi, T. Cheng, and D. Jiang. Quadratic convergence of Levenberg–Marquardt method for general nonlinear inverse problems with two parameters. *International Journal of Computer Mathematics*, 97(10):1949–1966, 2020.

[2] L. Banjai and F.-J. Sayas. *Integral Equation Methods for Evolutionary PDEs: A Convolution Quadrature Approach*. Springer, 2022.

[3] M. Bertero, P. Boccacci, and C. De Mol. *Introduction to Inverse Problems in Imaging*. CRC Press, 2021.

[4] A. Boulaouad, Y. Djenaihi, S. Boulaaras, H. Benseridi, and M. Dilmi. Study of a boundary value problem governed by the general elasticity system with a new boundary conditions in a thin domain. *Georgian Mathematical Journal*, 32(2):219–231, 2025.

[5] H.Brezis . *Functional Analysis, Sobolev Spaces and Partial Differential Equations*. Springer, New York, 2011.

[6] L. R. Evangelista and E. K. Lenzi. *An Introduction to Anomalous Diffusion and Relaxation*. Springer, Berlin/Heidelberg, Germany, 2023.

[7] W. Fan, X. Hu, and S. Zhu. Modelling, analysis, and numerical methods for a geometric inverse source problem in variable-order time-fractional subdiffusion. *Inverse Problems and Imaging*, 17(4):767–797, 2023.

[8] A. Giusti et al. On variable-order fractional linear viscoelasticity. *Mechanics of Time-Dependent Materials*. Springer, 2024.

[9] D.Henry. *Geometric Theory of Semilinear Parabolic Equations*. Springer, Berlin, 2006.

[10] Poincaré, Henri. Sur les équations aux dérivées partielles de la physique mathématique. *American Journal of Mathematics*, 12(3):211–294, 1890.

[11] J. Hadamard. Les problémes aux limites dans la théorie des équations aux dérivées partielles. *Journal de Physique Théorique et Appliquée*, 6(1):202–241, 1907.

[12] J. Hong and M. Yamamoto. Identification of a spatially-dependent variable order in one-dimensional subdiffusion. *SIAM Journal on Mathematical Analysis*, 57(2):1315–1341, 2025.

[13] V. Isakov. *Inverse Problems for Partial Differential Equations*. 3rd edition, Springer, 2017.

[14] X. Jin, S. Cai, H. Li, and G. E. Karniadakis. NSFnets (Navier–Stokes Flow Nets): Physics-informed neural networks for the incompressible Navier–Stokes equations. *Journal of Computational Physics*, 426:109951, 2021.

[15] B. Jin and Z. Zhou. Recovery of a space-time-dependent diffusion coefficient in subdiffusion: stability, approximation and error analysis. *IMA Journal of Numerical Analysis*, 43(4):2496–2531, 2023.

[16] J. B. Keller. Inverse problems. *The American Mathematical Monthly*, 83(2):107–118, 1976.

[17] K. J. Ford and M. M. Meerschaert. Space-time duality and high-order fractional diffusion. *Physical Review E*, 99(2):022122, 2019.

[18] Y. Kian, E. Soccorsi, and M. Yamamoto. On time-fractional diffusion equations with space-dependent variable order. *Annales Henri Poincaré*, 19(12):3855–3881, 2018.

[19] A. Kirsch. *An Introduction to the Mathematical Theory of Inverse Problems*. Vol. 120, Springer, New York, 2011.

[20] J. Lai et al. Investigation progresses and applications of fractional derivative model in geotechnical engineering. *Mathematical Problems in Engineering*, 2016(1):9183296, 2016.

[21] C. Li et al. One-dimensional consolidation of fractional order derivative viscoelastic saturated soils under arbitrary loading. *Chinese Journal of Geotechnical Engineering*, 39(5):895–902, 2017.

[22] C. Li et al. The application of a novel variable-order fractional calculus on rheological model for viscoelastic materials. *Mechanics of Advanced Materials and Structures*. Taylor & Francis, 2024.

[23] J. L. Lions and E. Magenes. *Non-Homogeneous Boundary Value Problems and Applications*, Volume II. Springer, Berlin, Heidelberg, 1972.

[24] Y. Liu. Numerical reconstruction of orders in coupled systems of subdiffusion equations. *International Conference Inverse Problems: Modelling and Simulation*. Springer Nature Switzerland, Cham, 2024.

[25] C. Lubich. Discretized fractional calculus. *SIAM Journal on Mathematical Analysis*, 17(3):704–719, 1986.

[26] C. Lubich. Convolution quadrature and discretized operational calculus. I. *Numerische Mathematik*, 52(2):129–145, 1988.

[27] Y. Luchko. Initial-boundary-value problems for the one-dimensional time-fractional diffusion equation. *Fractional Calculus and Applied Analysis*, 14(4):615–637, 2011.

[28] R. L. Magin. *Fractional Calculus in Bioengineering*. Begell House, 2006.

[29] D. Messaoudi, O. S. Ahmed, K. S. Agbodjan, T. Cheng, and D. Jiang. Numerical recovery of magnetic diffusivity in a three-dimensional spherical dynamo equation. *Inverse Problems & Imaging*, 14(5): 847–870, 2020.

[30] D. Messaoudi, T. Cheng, and D. Jiang. An augmented Lagrangian method for the identification of magnetic permeability in a Maxwell system. *Communications on Analysis and Computation*, 2(4):399–413, 2024.

[31] D. Messaoudi, M. Hemmal, and T. Abdelhamid. Simultaneous reconstruction of boundary coefficients in a parabolic system via regularized Levenberg–Marquardt optimization. *Gulf Journal of Mathematics*, 21(1):426–438, 2025.

[32] R. Metzler and J. Klafter. The random walk's guide to anomalous diffusion: a fractional dynamics approach. *Physics Reports*, 339(1):1–77, 2000.

[33] J. A. Nelder and R. Mead. A simplex method for function minimization. *The Computer Journal*, 7(4):308–313, 1965.

[34] A. A. Omar. *The Numerical Solution of Linear Variable Order Fractional Differential Equations Using Bernstein Polynomials*. Dissertation, Ministry of Higher Education, 2017.

[35] G. Pang, L. Lu, and G. E. Karniadakis. fPINNs: Fractional physics-informed neural networks. *SIAM Journal on Scientific Computing*, 41(4):A2603–A2626, 2019.

[36] M. Raissi, P. Perdikaris, and G. E. Karniadakis. Physics-informed neural networks: A deep learning framework for solving forward and inverse problems involving nonlinear partial differential equations. *Journal of Computational Physics*, 378:686–707, 2019.

[37] K. Sakamoto and M. Yamamoto. Initial value/boundary value problems for fractional diffusion-wave equations and applications to some inverse problems. *Journal of Mathematical Analysis and Applications*, 382(1):426–447, 2011.

[38] A. N. Tikhonov and V. Y. Arsenin. *Solutions of Ill-Posed Problems*. Winston and Sons, Washington, DC, 1977.

[39] P. Virtanen, R. Gommers, T. E. Oliphant, M. Haberland, T. Reddy, D. Cournapeau, E. Burovski, P. Peterson, W. Weckesser, J. Bright, et al. SciPy 1.0: Fundamental algorithms for scientific computing in Python. *Nature Methods*, 17(3):261–272, 2020.

[40] L. Wang and X. Li. Variable-order fractional damage creep model based on equivalent viscoelasticity for rock. *Rock and Soil Mechanics*, 42(1):117–128, 2021.

[41] K. Wu et al. Fractional viscoelastic solution of stratum displacement of a shallow tunnel under the surface slope condition. *Underground Space*, 8:123–138, 2023.

[42] Y. Xu et al. A Caputo variable-order fractional damage creep model for sandstone considering effect of relaxation time. *Acta Geotechnica*, 16(4):1025–1042, 2021.

[43] W. Henry ,Young. On classes of summable functions and their Fourier series. *Proceedings of the Royal Society of London. Series A, Containing Papers of a Mathematical and Physical Character*, 87(594):225–229, 1912.

[44] D. Yarotsky. Error bounds for approximations with deep ReLU networks. *Neural Networks*, 94:103–114, 2017.

[45] Q. Zhang and H. Liu. Mechanical analysis for the construction of deeply buried circular tunnels with liner in fractional Kelvin viscoelastic rock. *Chinese Quarterly of Mechanics*, 42(2):245–256, 2021.

Abstract

In this work, we study the inverse problem of identifying a space-dependent fractional order in a subdiffusion equation from observational data. The well-posedness of the forward problem is established, and the inverse problem is formulated using Tikhonov regularization. A finite element method combined with convolution quadrature is developed for the numerical approximation of the forward model, while a Physics-Informed Neural Network (PINN) approach is employed for the reconstruction of the unknown fractional order. Numerical results demonstrate the effectiveness of the proposed methods in one- and two-dimensional settings.

Keywords: *Inverse problems; Fractional diffusion equations; Tikhonov regularization; Finite element method; Convolution quadrature; Physics-Informed Neural Networks.*

Résumé

Dans ce travail, nous étudions le problème inverse consistant à identifier un ordre fractionnaire dépendant de l'espace dans une équation de sous-diffusion à partir de données d'observation. Le caractère bien posé du problème direct est établi, et le problème inverse est formulé à l'aide de la régularisation de Tikhonov. Une méthode des éléments finis combinée à une quadrature de convolution est développée pour l'approximation numérique du modèle direct, tandis qu'une approche basée sur les réseaux de neurones informés par la physique (PINNs) est utilisée pour la reconstruction de l'ordre fractionnaire inconnu. Les résultats numériques démontrent l'efficacité des méthodes proposées dans des cas unidimensionnels et bidimensionnels.

Mots-clés *: Problèmes inverses ; Équations de diffusion fractionnaire ; Régularisation de Tikhonov ; Méthode des éléments finis ; Quadrature de convolution ; Réseaux de neurones informés par la physique (PINNs*).

ملخص

في هذا العمل، ندرس المسألة العكسية المتمثلة في تحديد رتبة كسرية معتمدة على المكان في معادلة الانتشار الشاذ البطيء (Subdiffusion) انطلاقًا من بيانات الرصد. تم إثبات حسن الوضع للمسألة المباشرة، كما تمت صياغة المسألة العكسية باستخدام تنظيم تيخونوف (Tikhonov Regularization). وقد تم تطوير طريقة العناصر المحددة (Finite Element Method) مقترنةً بتربيع الالتفاف (Convolution Quadrature) من أجل التقريب العددي للنموذج المباشر، في حين استُخدمت مقاربة الشبكات العصبية المستنيرة بالفيزياء (Physics-Informed Neural Networks – PINNs) لإعادة بناء الرتبة الكسرية المجهولة. وتُظهر النتائج العددية فعالية الطرق المقترحة في الحالتين أحادية البعد وثنائية البعد.

الكلمات المفتاحية *: المسائل العكسية؛ معادلات الانتشار الكسرية؛ تنظيم تيخونوف؛ طريقة العناصر المحددة؛ تربيع الالتفاف؛ الشبكات العصبية المستنيرة بالفيزياء (PINNs).*